THE JOURNAL OF PHYSICAL CHEMISTRY B

pubs.acs.org/JPCB Article

Polariton-Mediated Electron Transfer via Cavity Quantum Electrodynamics

Arkajit Mandal,* Todd D. Krauss,* and Pengfei Huo*

Cite This: https://dx.doi.org/10.1021/acs.jpcb.0c03227 Read Online

ACCESS | Metrics & More | Article Recommendations | Supporting Information

ABSTRACT: We investigate the polariton-mediated electron transfer reaction in a model system with analytic rate constant theory and direct quantum dynamical simulations. We demonstrate that the photoinduced charge transfer reaction between a bright donor state and dark acceptor state can be significantly enhanced or suppressed by coupling the molecular system to the quantized radiation field inside an optical cavity. This is because the quantum light−matter interaction can influence the effective driving force and electronic couplings between the donor state, which is the hybrid light−matter excitation, and the molecular acceptor state. Under the resonance condition between the photonic and electronic excitations, the effective driving force can be tuned by changing the light−matter coupling strength; for an off-resonant condition, the same effect can be accomplished by changing the molecule−cavity detuning. We further demonstrate that using both the electronic coupling and light−matter coupling helps to extend the effective couplings across the entire system, even for the dark state that carries a zero transition dipole. Theoretically, we find that both the counter-rotating terms and the dipole self-energy in the quantum electrodynamics Hamiltonian are important for obtaining an accurate polariton eigenspectrum as well as the polariton-mediated charge transfer rate constant, especially in the ultrastrong coupling regime.

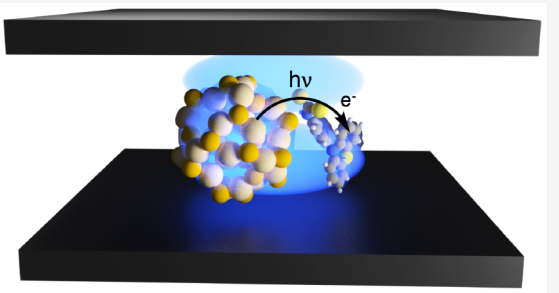

INTRODUCTION

Electron transfer (ET) reaction is one of the most ubiquitous and fundamental chemical reactions that plays a crucial role in a broad range of chemical processes. The equilibrium rate constant for the nonadiabatic ET reaction between the electronic donor and the acceptor states is given by the Marcus theory[1−3]

$$k_{ET} = \frac{{V_{DA}}^2}{\hbar}\sqrt{\frac{\pi\beta}{\lambda}}\exp\left[-\beta\frac{(\Delta G + \lambda)^2}{4\lambda}\right] \quad (1)$$

where ΔG is the ET driving force, λ is the reorganization energy, V_{DA} is the diabatic electronic coupling between the donor and acceptor electronic states, and $\beta = 1/k_B T$ (where k_B is the Boltzmann constant). This theory is enormously successful in predicting an accurate ET rate constant[4−9] when the reaction is in the nonadiabatic regime ($\beta V_{DA} \ll 1$) and when the reaction coordinate moves quasi-classically, such that the vibrational quantum effects[10−14] do not play an important role. Based on this simple theory, the charge transfer process can then be tuned by changing ΔG, λ, or V_{DA}.

It is of both the fundamental and practical interest to manipulate the charge transfer processes.[15] Interesting examples include (a) coupling the transfer of electron with a proton through proton-coupled electron transfer (PCET) reactions,[16−25] where the proton donor−acceptor vibronic wave function overlap modulates the diabatic electronic coupling, (b) fluctuating V_{DA} to mediate the charge transfer kinetics,[26−38] (c) using the temperature difference between the donor and acceptor to drive charge transfer,[39−41] (d) using infrared excitation to perturb ET,[42−44] (e) applying a strong electric field to induce stark effects to control charge transfer,[45−47] (f) using quantum interference effects to control ET,[48−53] (g) using electron bifurcation[54,55] to move electrons from a two-electron donor to spatially separated acceptors, and (h) using Auger-assisted processes to couple ET with hole excitation (or hole transfer with electron excitation).[56−59]

Coupling molecules to a quantized radiation field inside an optical cavity has recently shown to open up new paradigms of controlling photochemical reactivities.[60−63] Through the quantum light−matter interactions, the electronic states of molecules hybridize with the photonic states inside the cavity, generating a new set of photon-matter entangled states, so-called polaritons. The curvatures of these polaritonic potential energy surfaces can be engineered by tuning the frequency of the quantized radiation field[64−66] or the coupling strength of light−matter interactions,[64,66] thus opening up new possibilities to control chemical reactions by changing the fundamental

Received: April 10, 2020
Revised: June 23, 2020
Published: June 26, 2020

properties of the quantized radiation field inside an optical cavity.[64,65,67,68] Theoretical investigations play a crucial role in revealing the new principles in polariton photochemistry.[64,65,69,70] Recent theoretical studies have shown that coupling molecular systems to quantized radiation modes can suppress[71] or enhance[65,72] photoisomerization reactions,[66,71−73] modify potential energy landscapes even in the absence of any photon in the cavity,[65,71,74−76] increase charge transfer rate,[77−79] enhance electron−phonon coupling strength,[80] accelerate singlet fission kinetics,[81] control chemical reactions remotely,[82] enhance excitation energy transfer processes,[79,83,84] and create new conical intersections through light−matter interactions,[65,75,85,86] or split one existing electronic conical intersection into two polaritonic conical intersections.[87]

In this paper, we theoretically investigate the polariton-mediated electron transfer (PMET) reaction in a model molecular system coupled to the cavity. The molecular system contains a ground state, a bright donor state, and a dark acceptor state. To this end, we explore the possibilities of tuning the driving force ΔG, the electronic coupling V_{DA} or the reorganization energy λ by changing the properties of quantized radiation field inside the optical cavity, such as the light−matter coupling strength, by changing the frequencies of the photon (hence the detuning of the optical gap and electronic energies), or by changing the initial photonic-electronic quantum state. Unlike the previous theoretical work[77] that omits the presence of the dipole self-energy (DSE) or the counter-rotating terms (CRT), here, we explicitly explore the influence of both terms in PMET. We find that in the ultrastrong coupling (USC) regime[88] (defined as $0.1 < \eta < 1.0$, where $\eta = g_c/\omega_c$ is the ratio of the light−matter coupling strength and the photon frequency[88]), both terms play an important role in order to obtain an accurate polariton eigenspectrum and to accurately describe the PMET rate constant. With the current experimental setup, it is now possible to achieve the USC regime at the single quantum emitter limit.[89,90] Through direct quantum dynamical simulations and using analytic rate expressions, we demonstrate that the quantum light−matter interactions can significantly enhance or suppress the photoinduced charge transfer reactions by changing the polariton modified effective driving force, as well as the effective electronic coupling between the polaritonic donor state and acceptor state. This work provides a solid theoretical foundation to investigate PMET beyond the weak light−matter interaction regime, as well as demonstrates the possibilities to exploit intrinsic quantum behaviors of photons to tune charge transfer chemical reactions.

THEORETICAL APPROACHES

Model Hamiltonian. The molecule−cavity interaction is described by the quantum electric-dipole Hamiltonian, which is obtained from the Power-Zienau-Woolley (PZW) gauge transformation[91−93] of the minimal-coupling QED Hamiltonian in the Coulomb gauge. Further assuming the long-wavelength approximation[94] gives the Pauli−Fierz (PF) nonrelativistic QED Hamiltonian[94−96] which has been recently used to investigate cavity QED-mediated photochemistry.[69,96,97] The complete derivation of this Hamiltonian is provided in Appendix A.

The light−matter hybrid system based upon the PF QED Hamiltonian is described as follows

$$\hat{H} = \hat{H}_{en} + \hat{H}_{p} + \hat{H}_{enp} \tag{2}$$

where $\hat{H}_{en}$ is the electronic-nuclear Hamiltonian of the molecular system, $\hat{H}_{p}$ is the photonic Hamiltonian, and $\hat{H}_{enp}$ describes the quantum light−matter interactions between the molecules and the quantized field inside the cavity. Below, we briefly describe each part of the above Hamiltonian, then provide the polariton eigenspectrum calculated at different level of theories, and finally provide the expression of the rate constant for the polariton-mediated electron transfer (PMET) process.

Molecular Hamiltonian. The molecular Hamiltonian is modeled by a three-state system, with a ground state $|G\rangle$, an optically bright excited state denoted as the donor state $|D\rangle$, and an optically dark excited state, denoted as the acceptor state $|A\rangle$. These three states are treated as diabatic states in our model, based on considering that the electronic couplings between the $|G\rangle$ state and the excited states ($|D\rangle$ and $|A\rangle$ states) are assumed to be zero. Furthermore, $|D\rangle$ and $|A\rangle$ are coupled to each other through electronic couplings; thus, they are considered as excited diabatic states. The molecular Hamiltonian (electronic and nuclear part) is expressed as follows

$$\hat{H}_{en} = \hat{T}_{s} + \hat{H}_{e} + \hat{H}_{sb} \tag{3}$$

where $\hat{T}_{s} = \hat{P}_{s}^{2}/2m_{s}$ represents the kinetic energy operator of the reaction coordinate R_s (with mass m_s and frequency ω_s), $\hat{H}_e$ is the electronic Hamiltonian that describes the state-dependent part of $\hat{H}_{en}$, $\hat{H}_{sb}$ describes the interaction between the collective solvent coordinate R_s and a dissipative bath. With these three *diabatic* electronic states $|\alpha\rangle \in \{|G\rangle, |D\rangle, |A\rangle\}$, $\hat{H}_e$ can be expressed as

$$\hat{H}_{e} = \sum_{\alpha} U_{\alpha}|\alpha\rangle\langle\alpha| + V_{DA}(|D\rangle\langle A| + |A\rangle\langle D|) + \sum_{\alpha} \frac{1}{2} m_{s}\omega_{s}^{2}(R_{s} - R_{\alpha}^{0})^{2}|\alpha\rangle\langle\alpha| \tag{4}$$

Here, we assume that the diabatic surface for each state is a simple harmonic potential as a function of R_s centered around R_{α}^{0}. In addition, U_α represents a constant diabatic energy associated with state $|\alpha\rangle$, and V_{DA} is a constant diabatic electronic coupling between the excited donor and acceptor state. They have the following expressions

$$U_{\alpha} = \langle\alpha|\hat{H}_{e}(R_{\alpha}^{0})|\alpha\rangle;\ V_{DA} = \langle A|\hat{H}_{e}|D\rangle \tag{5}$$

The driving force ΔG for the ET reaction is

$$\Delta G = \langle A|\hat{H}_{e}(R_{A}^{0})|A\rangle - \langle D|\hat{H}_{e}(R_{D}^{0})|D\rangle = U_{A} - U_{D} \tag{6}$$

and the reorganization energy is[2,3]

$$\lambda = \frac{1}{2} m_{s}\omega_{s}^{2}(R_{A}^{0} - R_{D}^{0})^{2} \tag{7}$$

A physical system that we proposed here for $\hat{H}_{en}$ is the colloidal nanocrystal (NC) with an organic molecular acceptor,[56,57,98,99] which we plan to theoretically simulate with *ab initio* electronic structure calculations and experimentally investigate in future. NCs are advantageous in this application because they are well-established electron[56,99,100] and hole donors[57,98] with long excited state lifetimes and they have been coupled to several types of optical cavity,[101−103] and achieving the strong and ultrastrong coupling regimes under the single emitter limit is a promising ongoing research direction.[89,90,104] Furthermore, polaritonic photochemistry in such system is advantageous since the transition dipole moment between the ground and the

https://dx.doi.org/10.1021/acs.jpcb.0c03227
J. Phys. Chem. B XXXX, XXX, XXX−XXX

donor state is large and isotropic due to the spherical symmetry of the NC.[105] Therefore, regardless of the orientation of such NC system with respect to the field polarization direction, the quantized radiation modes and the NC always couple to each other. This is in contrast to other molecular systems where the rotation of the molecule changes the light−matter coupling strength and can create polariton induced conical intersection.[86,106]

In this work, we assume $R_G^0 = R_D^0 = 0$ to simplify our discussion. This is a reasonable assumption for the NC system, which has a small Huang−Rhys factor upon photoexcitation compared to molecular systems.[56,107,108] The effects of $R_G^0 \neq R_D^0$ is explored in the Supporting Information. Further, we choose $\lambda = 0.65$ eV, $T = 298$ K, and $V_{DA} = 5$ meV, and $R_A^0 = \sqrt{\frac{2\lambda}{m_s\omega_s^2}}$. These parameters are in agreement with the typical values of NC coupled to organic molecules.[56] In this work, the small electronic coupling ($\beta V_{DA} \ll 1$ where $\beta = 1/k_BT$), together with the quasi-classical behavior of R_s (due to its low frequency $\hbar\omega_s \ll k_BT$) and the short memory-time for the bath modes allow using the Marcus theory for obtaining an accurate rate constant. This is corroborated by the numerical results from our path-integral quantum dynamics simulations, which does not have these limitations in the Marcus theory and can provide accurate charge transfer rate constant.[109] In addition, we have explicitly ignored the electronic couplings between the ground state $|G\rangle$ and the excited states $|D\rangle$ or $|A\rangle$; we assume that the nonradiative decay from the excited states to the ground state occurs in a much longer time-scale compared to the PMET dynamics we investigated here.

The collective solvent coordinate R_s is coupled to a dissipative environment (phonon bath) modeled by the Caldeira−Leggett[110] system-bath Hamiltonian

$$\hat{H}_{sb} = \sum_k \left[\frac{P_k^2}{2m_k} + \frac{m_k\omega_k^2}{2}\left(R_k - \frac{c_k R_s}{m_k\omega_k^2}\right)^2 \right]$$

where R_k represents the k_{th} bath mode, with the mass m_k equal to m_s. The corresponding coupling constant c_k and the frequency ω_k are described by an ohmic spectral density $J(\omega) = \zeta\omega e^{-\omega/\omega_0}$, with a characteristic frequency $\omega_0 = 10\omega_s$ and a friction constant ζ. Note that the role of the system-bath Hamiltonian is purely fluctuating R_s, not causing any state-dependent energy shift. Further, the system-bath Hamiltonian does not impact the ET dynamics under the Markovian limit (short bath memory), and the parameters of ζ and ω_0 do not explicitly show up in the rate constant expression in eq 1. Hence, our results are independent of the particular choice of the parameters in the spectral density, as long as they are in the Markovian limit such that memory effects can be safely ignored.

The details of the parameters in $\hat{H}_{en}$ are provided in Table 1.

Table 1. Parameters Used for the Molecular System

parameter	value (unit)
β	298 (K)
ζ	25.789 (ps)
m_s	0.265 (ps^2)
ω_s	14.498 (ps^{-1})
λ	0.65 (eV)
V_{DA}	0.005 (eV)

Light-Matter Interaction Hamiltonian. The quantized radiation mode in the optical cavity is described as

$$\hat{H}_p = \hbar\omega_c\left(\hat{a}^\dagger\hat{a} + \frac{1}{2}\right) \tag{8}$$

where $\hat{a}^\dagger$ and $\hat{a}$ are the photonic creation and annihilation operators, with the frequency ω_c.

The NC−molecule subsystem is coupled to the radiation mode through the following interaction

$$\hat{H}_{enp} = \sqrt{\frac{\hbar\omega_c}{2\varepsilon_0\mathcal{V}}}\hat{\boldsymbol{\mu}}\cdot\hat{\boldsymbol{\epsilon}}(\hat{a}^\dagger + \hat{a}) + \frac{1}{2\varepsilon_0\mathcal{V}}(\hat{\boldsymbol{\mu}}\cdot\hat{\boldsymbol{\epsilon}})^2 \tag{9}$$

where $\hat{\boldsymbol{\mu}}$ is the total dipole operator of the NC−molecule system (electrons and nuclei), $\mathcal{V}$ is the effective quantization volume of the cavity, $\hat{\boldsymbol{\epsilon}}$ is the unit vector along the polarization direction of radiation mode (see Appendix A for details). Using the photonic coordinate $\hat{q} = \sqrt{\hbar/2\omega_c}(\hat{a}^\dagger + \hat{a})$ and momentum operator $\hat{p} = i\sqrt{\hbar\omega_c/2}(\hat{a}^\dagger - \hat{a})$, one can write down the light−matter interaction as follows

$$\hat{H}_p + \hat{H}_{enp} = \frac{1}{2}\hat{p}^2 + \frac{1}{2}\omega_c^2\left(\hat{q} + \frac{1}{\omega_c}\sqrt{\frac{1}{\varepsilon_0\mathcal{V}}}\hat{\boldsymbol{\mu}}\cdot\hat{\boldsymbol{\epsilon}}\right)^2$$

The second term in $\hat{H}_{enp}$ of eq 9 corresponds to the quadratic dipole self-energy (DSE), which has shown to be important in the USC regime of cavity QED.[94] The DSE term arises from the PZW transformation that explicitly mixes the electronic and photonic degrees of freedom.[69,94] This term describes how the polarization of the matter system acts back on the photon field,[69] which has not been extensively considered in polaritonic photochemistry. In a two-level system with no permanent dipole moment, this term causes a constant energy shift, and therefore can be ignored, as commonly done in the Jaynes−Cummings (JC) model or the Rabi model. However, beyond two-level systems, this term can cause *state-dependent* energy shifts and therefore can play an important role in the polaritonic quantum dynamics.

We assume that the NC−molecule subsystem is charge neutral, and the donor and acceptor electronic states do not possess any permanent dipole moment. We further assume that the transition dipole moment between the ground state and the optically dark acceptor state is zero, and the transition dipole between the donor and the acceptor state is also zero. This is because, for both $|D\rangle$ and $|G\rangle$ states, the transferring charge is confined on the NC, causing a large transition dipole between these two states. For the $|A\rangle$ state, the charge is localized on the acceptor molecule, which is spatially separated from the charge density of $|D\rangle$ and $|G\rangle$ state, resulting in nearly zero transition dipoles among them. This assumption is further validated by the experimental observations that no apparent optical transitions occur[56,99] from $|G\rangle$ to $|A\rangle$ or from $|D\rangle$ to $|A\rangle$. Under these simplifications, the dipole moment operator in the diabatic representation becomes $\hat{\boldsymbol{\mu}} = \boldsymbol{\mu}_{GD}(|D\rangle\langle G| + |G\rangle\langle D|)$, where $\boldsymbol{\mu}_{GD}$ is the transition dipole moment between the ground and the donor state. Thus, the projected dipole operator along the field polarization direction, $\hat{\mu} \equiv \hat{\boldsymbol{\mu}}\cdot\hat{\boldsymbol{\epsilon}}$ is expressed as follows

$$\begin{aligned}\hat{\mu} &\equiv \hat{\boldsymbol{\mu}}\cdot\hat{\boldsymbol{\epsilon}} = \boldsymbol{\mu}_{GD}\cdot\hat{\boldsymbol{\epsilon}}(|D\rangle\langle G| + |G\rangle\langle D|) \\ &\equiv \mu_0(|D\rangle\langle G| + |G\rangle\langle D|),\end{aligned} \tag{10}$$

https://dx.doi.org/10.1021/acs.jpcb.0c03227
J. Phys. Chem. B XXXX, XXX, XXX−XXX

where we have defined μ_0 through the above equation. The light−matter coupling in eq 9 is defined as

$$\hbar g_c \equiv \sqrt{\frac{\hbar\omega_c}{2\varepsilon_0 \mathcal{V}}}\boldsymbol{\mu}_{GD}\cdot\hat{\boldsymbol{\epsilon}} \equiv \sqrt{\frac{\hbar\omega_c}{2\varepsilon_0 \mathcal{V}}}\mu_0 \tag{11}$$

Note that in general, $\boldsymbol{\mu}_{GD}\cdot\hat{\boldsymbol{\epsilon}}$ depends on the nuclear coordinate and the orientation of transition dipole with respect to the cavity polarization mode. Here, this quantity is assumed to be independent of the nuclear coordinate as well as independent of the orientations of the dipole with respect to $\hat{\boldsymbol{\epsilon}}$ because of the isotropic transition dipole carried by the colloidal nanocrystal.

The light−matter interaction Hamiltonian $\hat{H}_{enp}$ in eq 9 for the model system is now expressed as

$$\begin{aligned}\hat{H}_{enp} &= \hbar g_c(|D\rangle\langle G| + |G\rangle\langle D|)(\hat{a}^\dagger + \hat{a}) + \hat{H}_{ds},\\ &\equiv \hbar g_c(\hat{\sigma}^\dagger + \hat{\sigma})(\hat{a}^\dagger + \hat{a}) + \hat{H}_{ds}\end{aligned} \tag{12}$$

where we have introduced the following excitation and de-excitation operators for the NC−molecule system

$$\hat{\sigma}^\dagger \equiv |D\rangle\langle G|;\ \hat{\sigma} \equiv |G\rangle\langle D| \tag{13}$$

It is easy to verify that $\hat{\sigma}^\dagger|G\rangle = |D\rangle\langle G|G\rangle = |D\rangle$, $\hat{\sigma}|D\rangle = |G\rangle$, and $\hat{\sigma}^\dagger|D\rangle = \hat{\sigma}|G\rangle = 0$, because $|D\rangle$ and $|G\rangle$ are orthogonal diabatic states.

The DSE operator $\hat{H}_{ds} = \frac{1}{2\varepsilon_0\mathcal{V}}(\hat{\boldsymbol{\mu}}\cdot\hat{\boldsymbol{\epsilon}})^2$ is expressed as

$$\begin{aligned}\hat{H}_{ds} &= \frac{1}{\hbar\omega_c}\left(\sqrt{\frac{\hbar\omega_c}{2\varepsilon_0\mathcal{V}}}\mu_0(|G\rangle\langle D| + |D\rangle\langle G|)\right)^2\\ &= \frac{\hbar g_c{}^2}{\omega_c}(|D\rangle\langle D| + |G\rangle\langle G|),\end{aligned} \tag{14}$$

with μ_0 and $\hbar g_c$ defined in eq 10 and eq 11, respectively. We further denote the above DSE as $\hbar\xi/2$ through the following definition

$$\hbar\xi = 2\hbar g_c{}^2/\omega_c \tag{15}$$

With the above terms, $\hat{H}_{enp}$ (eq 12) in eq 12 can now be expressed as

$$\begin{aligned}\hat{H}_{enp} &= \hbar g_c(|D\rangle\langle G| + |G\rangle\langle D|)(\hat{a}^\dagger + \hat{a})\\ &\quad + \frac{\hbar\xi}{2}(|D\rangle\langle D| + |G\rangle\langle G|)\end{aligned} \tag{16}$$

Note that because we assume $\mu_{GA} = 0$ and $\mu_{DA} = 0$ in our model, the photon-dressed acceptor state $|A, n\rangle$ does not carry the DSE, i.e., $\langle A, n|\hat{H}_{ds}|A, n\rangle = 0$; only the $|D, n\rangle$ and $|G, n\rangle$ states do.

Polaritonic Hamiltonian. We further define the polaritonic Hamiltonian $\hat{H}_{pl}$ as follows

$$\begin{aligned}\hat{H}_{pl} &= \hat{\mathcal{P}}\hat{H}_e\hat{\mathcal{P}} + \hat{H}_p + \hat{H}_{enp}\\ &= \hat{\mathcal{P}}\hat{H}_e\hat{\mathcal{P}} + \hbar\omega_c\left(\hat{a}^\dagger\hat{a} + \frac{1}{2}\right) + \hbar g_c(\hat{\sigma}^\dagger + \hat{\sigma})(\hat{a}^\dagger + \hat{a})\\ &\quad + \frac{\hbar\xi}{2}(|D\rangle\langle D| + |G\rangle\langle G|),\end{aligned} \tag{17}$$

where $\hat{H}_e$ (eq 4) is the electronic part of the Hamiltonian, $\hat{H}_p$ (eq 8) is the photonic Hamiltonian, and $\hat{H}_{enp}$ (eq 16) describes matter-field interactions. Note that we use the projection operator $\hat{\mathcal{P}} = |G\rangle\langle G| + |D\rangle\langle D|$ to confine $\hat{H}_e$ within the $\{|G\rangle, |D\rangle\}$ subspace. Thus, we do not consider the electronic acceptor state $|A\rangle$ in $\hat{H}_{pl}$, and only focus on the optically bright part of the Hamiltonian that spans in the subspace of $\{|G, n+1\rangle, |D, n\rangle\}$. Excluding the acceptor state also allows us to analytically obtain the eigenspectrum of $\hat{H}_{pl}$. We make this choice based on the fact that, in our model system, the acceptor states do not directly couple to the cavity through $\hat{H}_{enp}$ (eq 12) but only indirectly through the electronic coupling V_{DA}. This is a valid assumption when the electronic coupling is much smaller than the light−matter coupling strength, $V_{DA} \ll \hbar g_c$. When the electronic coupling is comparable or even larger than the light matter coupling, the acceptor state $|A, 0\rangle$ is coupled to the donor state $|D, 0\rangle$ through V_{DA}, and the donor state $|D, 0\rangle$ also couples to $|G, 1\rangle$ through the light−matter interaction $\hbar g_c$. Thus, the acceptor state is effectively coupled to the photonic excitation of the cavity $|G, 1\rangle$, even though the acceptor state does not carry any transition dipole. For this regime, direct quantum dynamics simulation is used to explore the polariton photochemical reactivities when all of these states are mixed. The idea of using both light−matter couplings and the electronic couplings can also be generalized to other NC−molecular systems that involve many NCs or acceptor molecules, such that the effective communications between the matter and the cavity can be extended across the entire hybrid systems.

Using the electronic-photonic basis $\{|\alpha, n\rangle\} = \{|\alpha\rangle \otimes |n\rangle\}$, eq 17 is expressed as

$$\begin{aligned}\hat{H}_{pl} &= \sum_{\alpha,n}\left[H_\alpha(R_s) + \left(n + \frac{1}{2}\right)\hbar\omega_c + \frac{\hbar\xi}{2}\right]|\alpha, n\rangle\langle\alpha, n|\\ &\quad + \sum_n \sqrt{n+1}\,\hbar g_c[|D, n\rangle\langle G, n+1| + |G, n+1\rangle\langle D, n|]\\ &\quad + \sum_n \sqrt{n+1}\,\hbar g_c[|G, n\rangle\langle D, n+1| + |D, n+1\rangle\langle G, n|]\end{aligned}$$

where $\{|\alpha\rangle\} \in \{|G\rangle, |D\rangle\}$ is the electronic states, $\{|n\rangle\}$ is the Fock state of the radiation mode, and $H_\alpha(R_s) = \langle\alpha|\hat{H}_e(R_s)|\alpha\rangle = 1/2m_s\omega_s{}^2(R_s - R_\alpha^0)^2 + U_\alpha$.

The eigenstate of $\hat{H}_{pl}$ is the so-called polariton state, which is obtained through the following eigenequation:

$$\hat{H}_{pl}|\Phi_\nu(R_s)\rangle = E_\nu(R_s)|\Phi_\nu(R_s)\rangle \tag{18}$$

The polariton states $|\Phi_\nu(R)\rangle$ can be expressed as linear combinations of the exciton-Fock basis as follows:

$$|\Phi_\nu(R_s)\rangle = \sum_{\alpha,n} c_{\alpha n}^\nu(R_s)|\alpha, n\rangle \tag{19}$$

The polariton energies and eigenvectors can be obtained by numerically diagonalizing $\hat{H}_{pl}$'s matrix under the $\{|\alpha,n\rangle\}$ basis, or exactly[111,112] as explained in the next section.

The energy detuning between $|G, n+1\rangle$ and $|D, n\rangle$ states is

$$\hbar\delta\omega_c(R_s) = \hbar\Delta\omega_c + \frac{1}{2}m_s\omega_s{}^2[(R_s - R_G^0)^2 - (R_s - R_D^0)^2] \tag{20}$$

where $\Delta\omega_c$ represents the electronic-photonic detuning

$$\Delta\omega_c = \omega_c - (U_D - U_G)/\hbar \tag{21}$$

and the second term in eq 20 represents the detuning contribution from the vibronic coupling difference between the $|G\rangle$ and $|D\rangle$ states, which leads to the "polaron decoupling effect" mediated by the cavity.[77] We have explored the same

https://dx.doi.org/10.1021/acs.jpcb.0c03227
J. Phys. Chem. B XXXX, XXX, XXX−XXX

effect through direct quantum dynamics simulations, with the results provided in the Supporting Information. For all of the results presented in the main text, we assume that $R_G^0 = R_D^0 = 0$, which leads to $\hbar\delta\omega_c = \hbar\Delta\omega_c$.

Figure 1 presents a schematic illustration of the model system considered in this work. Here, the "matter" part of the system

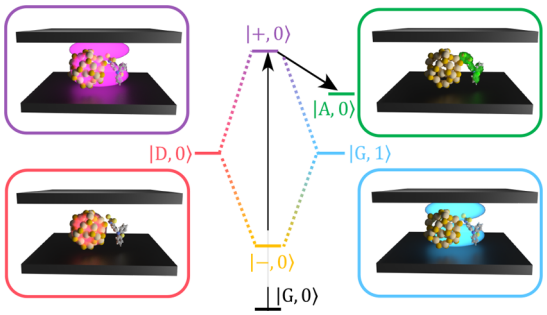

Figure 1. Schematic illustrations of the polariton-mediated electron transfer process. Here, $|G, 0\rangle$ represents the ground states of the NC−molecule−cavity hybrid system; $|D, 0\rangle$ (red) represents the electronic excitation on the donor, with 0 photons in the cavity; $|A, 0\rangle$ (green) represents the electronic excitation on the acceptor, with 0 photons in the cavity; $|G, 1\rangle$ (blue) represents the ground states of the NC−molecule system, with 1 photon inside the cavity. Through the molecule−cavity interactions, $|D, 0\rangle$ and $|G, 1\rangle$ hybridize to generate the polariton states $|+, 0\rangle$ (magenta) and $|-, 0\rangle$ (yellow).

contains a colloidal nanocrystal (NC) plus an organic acceptor molecule.[104] Note that the figure is out of proportion for the size of the cavity and NC. The actual size of the NC[56] is around 2 nm. The quantized distance in the FP cavity, on the other hand, is ∼210 nm for $\hbar\omega_c = 3.0$ eV. Thus, for the NC (and the attached molecule), the quantized field (as well as the vector potential) can be viewed as a constant field, making the long-wavelength approximation valid in the electric-dipole Hamiltonian (see Appendix A). The photon-dressed state $|D, 0\rangle$ (red, electronic excitation on the NC donor and 0 photons in the cavity) and $|G, 1\rangle$ (blue, 1 photon in the cavity and ground state for the NC−molecule) hybridize to form the polariton state $|+, 0\rangle$ (magenta) and $|-, 0\rangle$ (yellow), corresponding to the superposition of excitation on both the matter and the quantized field. The optically bright states for the matter-cavity hybrid systems are these polariton states.[60,67] Through the quantum light−matter interactions, the energies of the $|+, 0\rangle$ and $|-, 0\rangle$ state are split by the amount of $\hbar\Omega_R$. Hence, they are shifted relative to the energy of the acceptor state $|A, 0\rangle$ (which is not coupled to the cavity due to $\boldsymbol{\mu}_{GA} = 0$). Thus, the effective electronic driving force from the polariton states ($|+, 0\rangle$ or $|-, 0\rangle$) to the acceptor state $|A, 0\rangle$ (green, the electron transferred to the molecule) can be tuned, significantly influencing the charge transfer dynamics.

Polariton Eigenspectrum. So far, we have not introduced any approximation in the Hamiltonian (eq 2), except for the long-wavelength approximation that allows one to derive the PF Hamiltonian (see Appendix A) and the single mode approximation for the cavity. Below, we outline various approaches to obtain the polariton eigenspectrum. The polariton Hamiltonian $\hat{H}_{pl}$ in eq 17 (in the Pauli−Fierz form) contains the DSE term. Dropping this term gives the so-called Rabi model Hamiltonian:

$$\begin{aligned}\hat{H}_{Rabi} &= \hat{H}_{pl} - \hat{H}_{ds} \\ &= \hat{\mathcal{P}}\hat{H}_e\hat{\mathcal{P}} + \hbar\omega_c\left(\hat{a}^\dagger\hat{a} + \frac{1}{2}\right) + \hbar g_c(\hat{\sigma}^\dagger + \hat{\sigma})(\hat{a}^\dagger + \hat{a})\end{aligned} \tag{22}$$

The Rabi model can be solved exactly by using the Bargmann transformation[111,113] or by using Bogoliubov transformations.[112] The eigenvalues are the roots of a transcendental function (Henu function) which does not have analytic expressions. Nevertheless, the same approach can be used to exactly solve the Polariton Hamiltonian $\hat{H}_{pl}$ (eq 17) in our case, because the dipole self-energy contribution considered here only involves a constant energy shift (eq 14).

To obtain analytic expressions of the polariton eigenspectrum, we begin with the most commonly used rotating wave approximation (RWA) that ignores the $|G\rangle\langle D|\hat{a} \equiv \hat{\sigma}\hat{a}$ and $|D\rangle\langle G|\hat{a}^\dagger \equiv \hat{\sigma}^\dagger\hat{a}^\dagger$ terms in $\hat{H}_{enp}$ (eq 12). We denote the counter-rotating (CR) Hamiltonian as

$$\hat{H}_{pl}^{(1)} = \hbar g_c(|D\rangle\langle G|\hat{a}^\dagger + |G\rangle\langle D|\hat{a}) = \hbar g_c(\hat{\sigma}^\dagger\hat{a}^\dagger + \hat{\sigma}\hat{a}) \tag{23}$$

The RWA Hamiltonian is thus defined as

$$\begin{aligned}\hat{H}_{pl}^{(0)} &= \hat{H}_{pl} - \hat{H}_{pl}^{(1)} \\ &= \hat{\mathcal{P}}\hat{H}_e\hat{\mathcal{P}} + \hbar\omega_c\left(\hat{a}^\dagger\hat{a} + \frac{1}{2}\right) + \hbar g_c(\hat{\sigma}^\dagger\hat{a} + \hat{\sigma}\hat{a}^\dagger) \\ &\quad + \frac{\hbar\xi}{2}(|D\rangle\langle D| + |G\rangle\langle G|)\end{aligned} \tag{24}$$

where $\hat{H}_{pl}$ is defined in eq 17. This allows one to easily obtain the analytical solution of the polariton eigenspectrum. Further dropping the DSE term under the RWA, the polariton Hamiltonian reduces to the so-called Jaynes−Cummings (JC) Hamiltonian

$$\begin{aligned}\hat{H}_{JC} &= \hat{H}_{pl} - \hat{H}_{pl}^{(1)} - \hat{H}_{ds} = \hat{H}_{pl}^{(0)} - \hat{H}_{ds} \\ &= \hat{\mathcal{P}}\hat{H}_e\hat{\mathcal{P}} + \hbar\omega_c\left(\hat{a}^\dagger\hat{a} + \frac{1}{2}\right) + \hbar g_c(\hat{\sigma}^\dagger\hat{a} + \hat{\sigma}\hat{a}^\dagger),\end{aligned} \tag{25}$$

which has been widely employed in quantum optics and molecular cavity-QED applications.[63,70,77,81,114,115] In the quantum optics literature, the JC model is obtained by dropping counter-rotating terms (CRTs) in the Rabi model, with the Hamiltonian $\hat{H}_{JC} = \hat{H}_{Rabi} - \hat{H}_{pl}^{(1)}$.

The cavity QED literature[116] often characterizes the coupling strength by using

$$\eta = \frac{g_c}{\omega_c} = \mu_0/\sqrt{2\varepsilon_0\mathcal{V}\hbar\omega_c} \tag{26}$$

Based on the value of η, the light−matter interaction can be roughly characterized as the weak to strong coupling regime[150] for the range of $0 \le \eta < 0.1$, ultrastrong coupling (USC)[88] regime when $0.1 \le \eta < 1$, and deep strong coupling (DSC)[116] regime $1 \le \eta$. In both the USC and DSC regimes, the DSE has to be included in order to get the correct polariton eigenenergy.[94] In this paper, we will focus on the case of weak, strong, and some part of the USC regime within the range of $0 \le \eta < 0.5$.

For a single molecule polariton Hamiltonian with a small light−matter coupling ($g_c \ll \omega_c$), the DSE term becomes less important ($\hbar\xi \ll \hbar g_c$), and both the PF and the JC Hamiltonian predict nearly identical results for polariton eigenenergy and the

https://dx.doi.org/10.1021/acs.jpcb.0c03227
J. Phys. Chem. B XXXX, XXX, XXX−XXX

polariton quantum dynamics. However, the DSE term should be included in order to guarantee a bounded ground state of the molecule−cavity hybrid system.[94] Without DSE, the Gauge invariance between the minimal coupling Hamiltonian and the electric-dipole Hamiltonian will breakdown. Further, in the recently emerged "ultra-strong" coupling regime between light and matter,[88] these DSE terms play a crucial role. For example, in an experimental work of using collective effects in molecular dielectric material for ultrastrong vibrational coupling, Ebbesen and co-workers have shown that these terms are necessary in the polariton model Hamiltonian in order to reproduce the polaritonic dispersion results in their experiments.[117] In the intersubband polaritonic systems[118,119] as well as a cavity QED model,[120] it has also been shown that DSE is necessary to be included to provide the correct equation of motion of the polaritonic state. Recently experiments with single quantum dot coupled to the cavity have also made impressive progress approaching toward the USC regime.[89,90]

The RWA starts to break down beyond the strong coupling regime. There are many available approaches to provide corrections, including the generalized RWA by choosing the proper basis before carrying the RWA[121,122] or mapping the Rabi model onto a solvable JC-like model by choosing a variational parameter and omitting multiphoton processes.[123] Here, we use a simple perturbation theory[124] that treats $\hat{H}_{\rm pl}^{(0)}$ as the 0th order Hamiltonian and $\hat{H}_{\rm pl}^{(1)}$ as the perturbation. This is a conceptually simple approach and it provides accurate enough results for the range of the coupling investigated here. Below, we elaborate on these different theoretical treatments, with a brief summary provided in Table 2.

Table 2. Various Levels of Theory (Approximation) Used for Solving the Eigenspectrum of $\hat{H}_{\rm pl}$

level of theory	Hamiltonian	eq
Jaynes−Cummings (JC)	$\hat{H}_{\rm JC}$	25
RWA	$\hat{H}_{\rm pl}^{(0)}$	24
perturbation theory (PT)	$\hat{H}_{\rm pl}^{(0)}$ and $\hat{H}_{\rm pl}^{(1)}$	23 and 24
Rabi	$\hat{H}_{\rm Rabi}$	22
Pauli−Fierz (PF)	$\hat{H}_{\rm pl}$	17

Rotating Wave Approximation. We start with the commonly used RWA which ignores the $\hat{\sigma}\hat{a}$ and $\hat{\sigma}^{\dagger}\hat{a}^{\dagger}$ terms in $\hat{H}_{\rm enp}$ (eq 12). Under this approximation, the RWA Hamiltonian $\hat{H}_{\rm pl}^{(0)}$ (eq 24) can be exactly diagonalized in the 2×2 subspace of $\{|{\rm G}, n+1\rangle, |{\rm D}, n\rangle\}$, giving the following polariton states

$$
\begin{aligned}
|+, n\rangle &= \sin\theta_{\rm c}|{\rm D}, n\rangle + \cos\theta_{\rm c}|{\rm G}, n+1\rangle \\
|-, n\rangle &= \cos\theta_{\rm c}|{\rm D}, n\rangle - \sin\theta_{\rm c}|{\rm G}, n+1\rangle,
\end{aligned} \tag{27}
$$

where the light−matter mixing angle $\theta_{\rm c}$ is expressed as follows

$$
\theta_{\rm c}(n) = \frac{1}{2}\tan^{-1}\left(\frac{2\sqrt{n+1}\,g_{\rm c}}{\Delta\omega_{\rm c}}\right) \tag{28}
$$

Under the RWA, the ground state $|{\rm G}, 0\rangle$ is decoupled from the rest of the states. Note that the presence of DSE does not change the above eigenfunction in our model system, because it only brings a constant energy shift for both $|{\rm G}, n+1\rangle$ and $|{\rm D}, n\rangle$ states. The energy of the photon-dressed acceptor state, on the other hand, does not contain the DSE due to the zero transition dipole assumed in our model. The DSE term plays an important role in reducing the divergence in the Lamb shift calculations[91,93] in the electric-dipole Hamiltonian. Here, we find it might play an interesting role in the PMET process in the USC regime.

The energy of the $|{\rm D}, n\rangle$ state is

$$
\begin{aligned}
E_{{\rm D},n} &= \langle {\rm D}, n|\hat{H}_{\rm pl}|{\rm D}, n\rangle \\
&= \frac{1}{2}m_{\rm s}\omega_{\rm s}^{\,2}R_{\rm s}^{\,2} + U_{\rm D} + \left(n+\frac{1}{2}\right)\hbar\omega_{\rm c} + \frac{\hbar\xi}{2},
\end{aligned} \tag{29}
$$

and the energy of the $|{\rm G}, n+1\rangle$ state is

$$
\begin{aligned}
E_{{\rm G},n+1} &= \langle {\rm G}, n+1|\hat{H}_{\rm pl}|{\rm G}, n+1\rangle \\
&= \frac{1}{2}m_{\rm s}\omega_{\rm s}^{\,2}R_{\rm s}^{\,2} + U_{\rm G} + \left(n+\frac{3}{2}\right)\hbar\omega_{\rm c} + \frac{\hbar\xi}{2}.
\end{aligned} \tag{30}
$$

The corresponding eigenenergies of these polariton states (under the RWA) are

$$
E_{\pm,n}^{(0)} = E_{{\rm D},n} + \frac{1}{2}\hbar\Delta\omega_{\rm c} \pm \frac{\hbar}{2}\Omega_{\rm R} \tag{31}
$$

where $E_{{\rm D},n}$ is defined in eq 29, $\hbar\Delta\omega_{\rm c}$ is defined in eq 21, and the Rabi-splitting $\Omega_{\rm R}$ is

$$
\Omega_{\rm R}(n) = \sqrt{\Delta\omega_{\rm c}^{\,2} + 4(n+1)g_{\rm c}^{\,2}} \tag{32}
$$

We emphasize that in the context of the molecular polariton, eq 31 does not represent "energy levels", but rather "potential energy surfaces"[64] as they are explicit functions of nuclear coordinate $R_{\rm s}$. Further ignoring the dipole self-energy operator (by setting $\hbar\xi = 0$) in the RWA Hamiltonian $\hat{H}_{\rm pl}^{(0)}$ (eq 24) leads to the commonly used Jaynes−Cummings (JC) Hamiltonian $\hat{H}_{\rm JC}$ (eq 25). The eigenenergies of $\hat{H}_{\rm JC}$ can be obtained as eq 31 with $\hbar\xi = 0$.

Perturbative Corrections. Furthermore, we use the RWA Hamiltonian $\hat{H}_{\rm pl}^{(0)}$ in eq 24 (which we know how to solve exactly) as the 0th order Hamiltonian and treat the CRT in $\hat{H}_{\rm pl}^{(1)}$ (eq 23) as the perturbation. The correction of the polariton eigenspectrum is calculated up to the second-order. Our main interest in this paper is the charge transfer dynamics from the $|\pm, 0\rangle$ states to $|{\rm A}, 0\rangle$ state. Thus, we will only focus on the lowest three polaritonic states. For the $|{\rm G}, 0\rangle$ state, the first-order correction is $E_{{\rm G},0}^{(1)} = \langle {\rm G}, 0|\hat{H}_{\rm pl}^{(1)}|{\rm G}, 0\rangle = \hbar g_{\rm c}\langle {\rm G}, 0|\hat{\sigma}^{\dagger}\hat{a}^{\dagger} + \hat{\sigma}\hat{a}|{\rm G}, 0\rangle = 0$. In addition, we notice that for the coupling $\langle k|\hat{H}_{\rm pl}^{(1)}|{\rm G}, 0\rangle = \hbar g_{\rm c}\langle k|\hat{\sigma}^{\dagger}\hat{a}^{\dagger} + \hat{\sigma}\hat{a}|{\rm G}, 0\rangle$, the only nonzero matrix elements are those with $\langle k| = \langle \pm, 1|$, such that $\langle \pm,1|\hat{\sigma}^{\dagger}\hat{a}^{\dagger} + \hat{\sigma}\hat{a}\,|{\rm G}, 0\rangle = \langle \pm, 1|{\rm D}, 1\rangle$. This leads to the second order correction of the ground state energy as

$$
\begin{aligned}
E_{{\rm G},0}^{(2)} &= \sum_{k\neq {\rm G},0}\frac{|\langle k|\hat{H}_{\rm pl}^{(1)}|{\rm G}, 0\rangle|^2}{E_{{\rm G},0}^{(0)} - E_k^{(0)}} \\
&= \frac{|\langle +, 1|\hat{H}_{\rm pl}^{(1)}|{\rm G}, 0\rangle|^2}{E_{{\rm G},0} - E_{+,1}} + \frac{|\langle -, 1|\hat{H}_{\rm pl}^{(1)}|{\rm G}, 0\rangle|^2}{E_{{\rm G},0} - E_{-,1}} \\
&= -\frac{\hbar g_{\rm c}^{\,2}}{2\omega_{\rm c}}\left[\frac{2\hbar\omega_{\rm c} + \hbar\Delta\omega_{\rm c}}{2\hbar\omega_{\rm c} + \hbar\Delta\omega_{\rm c} - \frac{\hbar}{\omega_{\rm c}}g_{\rm c}^{\,2}}\right].
\end{aligned} \tag{33}
$$

For the $|\pm, 0\rangle$ states, the first-order energy correction is $E_{+,0}^{(1)} = \langle +, 0|\hat{H}_{\rm pl}^{(1)}|+, 0\rangle = \hbar g_{\rm c}\langle +, 0|(\hat{\sigma}^{\dagger}\hat{a}^{\dagger}+\hat{\sigma}\hat{a})(\sin\theta_{\rm c}(0)|{\rm D}, 0\rangle + \cos\theta_{\rm c}(0)|{\rm G}, 1\rangle) = 0$, and similarly, $E_{-,0}^{(1)} = 0$. The coupling matrix elements are $\langle k|\hat{H}_{\rm pl}^{(1)}|+, 0\rangle = \hbar g_{\rm c}\langle k|(\hat{\sigma}^{\dagger}\hat{a}^{\dagger}+\hat{\sigma}\hat{a})(\sin\theta_{\rm c}(0)|{\rm D}, 0\rangle + \cos\theta_{\rm c}(0)|$

https://dx.doi.org/10.1021/acs.jpcb.0c03227
J. Phys. Chem. B XXXX, XXX, XXX−XXX

G, 1⟩) = $\hbar g_c \cos\theta_c(0)\langle k|\mathrm{D}, 2\rangle$, indicating that the only nonzero elements are those with $\langle k| = \langle \pm, 2|$. With these information, the second-order energy corrections can be shown as follows

$$E^{(2)}_{+,0} = -\frac{\hbar {g_c}^2}{\omega_c}\cos^2\theta_c(0)\left[\frac{2\hbar\omega_c - \frac{\hbar}{2}\Omega_R(0) + \frac{\hbar}{2}\Delta\omega_c}{2\hbar\omega_c - \hbar\Omega_R(0) - \frac{\hbar}{\omega_c}{g_c}^2}\right],$$

$$E^{(2)}_{-,0} = -\frac{\hbar {g_c}^2}{\omega_c}\sin^2\theta_c(0)\left[\frac{2\hbar\omega_c + \frac{\hbar}{2}\Omega_R(0) + \frac{\hbar}{2}\Delta\omega_c}{2\hbar\omega_c + \hbar\Omega_R(0) - \frac{\hbar}{\omega_c}{g_c}^2}\right], \quad (34)$$

where both the mixing angle $\theta_c(n)$ (eq 28) and the Rabi splitting $\Omega_R(n)$ (eq 32) in the above expressions are evaluated with $n = 0$ photons. The detailed derivations of the above energy corrections in eqs 33 and 34 are provided in the Supporting Information.

In quantum optics, the energy shift due to the CRT is commonly referred to as the Bloch−Siegert shift.[123,125] Note that under the resonance condition ($\hbar\Delta\omega_c = 0$ and $\cos\theta_c = \sin\theta_c = 1/\sqrt{2}$) as well as when $g_c/\omega_c < 1$, these second-order corrections of $E^{(2)}$ are of the same order of magnitude as $-\hbar {g_c}^2/2\omega_c = -\hbar\xi/4$. In comparison, the DSE contributes $+\hbar\xi/2$, which is roughly twice of the Bloch−Siegert shift, with an opposite sign. One can easily see that without DSE, the eigenenergy of polariton becomes unbounded. The DSE thus plays a crucial role to make sure a bounded ground state.[95] Therefore, both the CRT correction and the DSE term are important and must be included, especially in the USC regime. The Rabi model, which only considers the CRT but not the DSE, often leads to a larger deviation of the eigenenergy compared to the exact results.[126] The JC model Hamiltonian, which ignores both CRT corrections and DSE, could potentially provide even more accurate eigenenergy compared to the Rabi model.[126]

The first-order correction for the polaritonic state is

$$|\pm, 0\rangle^{(1)} = \sum_{k\neq\pm 0}\frac{\langle k|\hat{H}^{(1)}_{pl}|\pm, 0\rangle}{E_{\pm,0} - E_k}|k\rangle = c_+|+, 2\rangle + c_-|-, 2\rangle \quad (35)$$

with only nonzero contributions from those $\langle k| = \langle \pm, 2|$ as we discussed when calculating $E^{(2)}_{+,0}$ (see the paragraph above eq 34).

Exact Solution of the PF Hamiltonian. The exact solution of the Rabi Hamiltonian $\hat{H}_{Rabi}$ (eq 22) was first discovered by Braak[111] by noticing that the parity symmetry in the Rabi model is sufficient to solve the Hamiltonian exactly using bosonic operators in the Bargmann space.[111] Later, it was shown that the same solution can also be obtained from the Bogoliubov transformation.[112] Because the DSE in $\hat{H}_{pl}$ only involves a constant energy shift of $\hat{H}_{Rabi}$, we can directly borrow the exact solution of the Rabi model and write down the eigenenergy of $\hat{H}_{pl}$. In the work of Braak,[111] an essential component of the exact eigenspectrum is the root $x_{\pm,n}$ of the following equation[111,112]

$$\sum_{n=0}^{\infty} K_n(x_{\pm,n})\left[1 \mp \frac{\Delta\omega_c/2}{x_{\pm,n} - n\omega_c}\right]\left(\frac{g_c}{\omega_c}\right)^n = 0 \quad (36)$$

where $K_n(x)$ satisfies the recursive relation $nK_n = f_{n-1}K_{n-1} - K_{n-2}$, and $f_n(x) = \frac{2g_c}{\omega_c} + \frac{1}{2g_c}\left(n\omega_c - x + \frac{(\Delta\omega_c/2)^2}{x - n\omega_c}\right)$, with the initial condition $K_0 = 1$ and $K_1(x) = f_0(x)$. The exact eigenvalues of $\hat{H}_{Rabi}$ are $E_{\pm,n} = E_{D,n} + \hbar x_{\pm,n} - \frac{\hbar {g_c}^2}{\omega_c}$ with $\pm$ indicating the parity of the solution. Note that $E_{D,n}$ contains the dipole self-energy $\hbar\xi/2 = \hbar {g_c}^2/\omega_c$, which exactly cancels the corresponding negative term in $E^{ex}_{\pm,n}$.

Using these results, the exact eigenvalues of $\hat{H}_{pl}$ are

$$E^{ex}_{\pm,n} = E_{D,n} + \hbar x_{\pm,n} \quad (37)$$

with $E_{D,n}$ (which contains the dipole self-energy $\hbar\xi/2 = \hbar {g_c}^2/\omega_c$) defined in eq 29 and $x_{\pm,n}$ is the solution of eq 36. These are nonexceptional solutions.[111] All of the other exceptional eigenvalues[111] are $E^{ex}_n = E_{D,n} + n\hbar\omega_c$, under the condition $K_n(n\omega_c) = 0$.

Alternatively, the polariton Hamiltonian $\hat{H}_{pl}$ can be solved by direct diagonalization of the matrix under the electronic−Fock basis (electron-photon basis) $\{|\alpha,n\rangle\}$, with a sufficiently large Fock basis. It can also be solved by using the extended coherent states basis which includes many-body correlations through infinitely many photons in the cavity mode (and it is particularly useful in the strong coupling regime).[85] These schemes all generate identical numerical results for the lowest three states of $\hat{H}_{pl}$.

Numerical Results. Figure 2 presents three polariton eigenenergies at $R_s = 0$ shifted by the zero point energy of the photon, $1/2\hbar\omega_c$. They correspond to three polariton states |G, 0⟩, |−, 0⟩ and |+, 0⟩. Figure 2a presents the polaritonic eigenvalues as a function $\eta = g_c/\omega_c$ at $\hbar\Delta\omega_c = 0$ (resonance condition). Figure 2b presents the polaritonic eigenvalues as a function of the detuning $\hbar\Delta\omega_c$ with a light−matter coupling strength $\hbar g_c = 1$ eV. The eigenenergies are obtained at various levels theory (see Table 2), including the JC model (yellow) in eq 25 that ignores both CRT and DSE, the RWA Hamiltonian

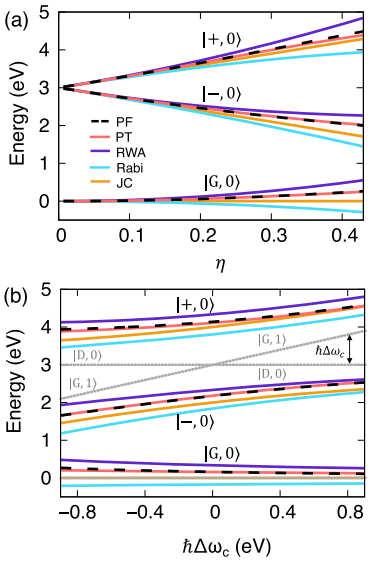

Figure 2. Polariton eigenspectrum of the model system with $R_s = 0$, (a) as a function of $\eta = g_c/\omega_c$ at $\hbar\Delta\omega_c = 0$ and (b) as a function of the detuning $\hbar\Delta\omega_c$ (see eq 21 and indicated in this panel) at $\hbar g_c = 1.0$ eV obtained with various levels of theory, including exact solution of PF Hamiltonian (black dashed), JC Hamiltonian (yellow) that assumes RWA and ignores DSE, Rabi Hamiltonian (cyan) that ignores DSE, RWA (magenta) that ignores counter rotating term (CRT), and Perturbation theory (PT) (red) which treats CRT perturbatively. These different level of theories are summarized in Table 2.

https://dx.doi.org/10.1021/acs.jpcb.0c03227
J. Phys. Chem. B XXXX, XXX, XXX−XXX

(magenta) in eq 24 that ignores the CRT, the Rabi model (cyan) in eq 22 that ignores the DSE, and the full PF treatment (black dashed) that includes both the CRT term and DSE. The perturbation theory (PT) (red) which treat CRT perturbatively and include the exact DSE provides very accurate polariton eigenvalue in the range of the parameter regime investigated here.

In the JC model Hamiltonian (yellow), the ground state does not shift by increasing η, while the $|+, 0\rangle$ and $|-, 0\rangle$ states linearly split as a function of η. This behavior can be easily understood by examining the JC eigenspectrum in eq 31. The Rabi model (cyan) which only accounts for the CRT, overestimates the negative energy corrections and incorrectly decreases energies for all states. Thus, the Rabi model predicts that the ground state energy becomes unstable. The RWA Hamiltonian (magenta) that ignores the CRT, but includes the DSE, overestimates the energy correction in the positive direction and shifts all states up. The perturbative treatment (red) that includes CRT as perturbation as well as the DSE performs well and is nearly identical with the exact PF curve within the range of the η or $\hbar\Delta\omega_c$ presented here. Note that in Figure 2b, for $\hbar\Delta\omega_c < -0.5$ eV, the polariton eigenenergy for $|-, 1\rangle$ becomes lower than that for $|+, 0\rangle$. As a result, a trivial crossing is formed between the third and fourth polaritonic eigenenergies as a function of $\hbar\Delta\omega_c$ at $\hbar\Delta\omega_c \approx -0.5$ eV. For simplicity, these polaritonic eigenenergies are presented in the Supporting Information and are not shown here.

From these numerical results, one can see that the overall contribution from the combined DSE and CRT is positive, as PF curves lie above the JC curves for all three polariton states. These results agree with our previous analysis that the CRT roughly contributes $-\hbar\xi/4$, partially compensating the positive shift caused by DSE which is exactly $\hbar\xi/2$. We emphasize that the PMET rate constant is exponentially sensitive to the driving force, which directly depends upon the polariton eigenenergies. Hence, a seemingly small deviation of the polariton energy obtained from various theoretical treatments can cause a large quantitative difference in the PMET rate constant (up to an order of magnitude, as shown in our numerical simulations). Thus, it is crucial to carefully include all contributions in the light−matter interactions for an accurate PMET rate.

Polariton Mediated Electron Transfer. For the bare molecular system (quantum dot plus the molecule), we assume that the photoexcitation leads to a Franck−Condon transition from the ground state $|G\rangle$ to the optically bright donor state $|D\rangle$. For a molecular system, FC approximation is valid for excitations among electronic states when using a short incident laser pulse to excite the system. Similarly, for a molecule−cavity hybrid system, FC is also valid for excitations among polaritonic states, when using a short incident laser pulse to excite the hybrid system as assumed in this work. Since both $|D\rangle$ and $|G\rangle$ are centered around $R_s = 0$ in our model system, the photoexcitation leads to an *equilibrium* initial condition for the nuclear distribution, which allows using the Marcus ET rate expression in eq 1.

For the NC−molecule−cavity hybrid system, we are interested in the ET rate from $|+, 0\rangle$ (or $|-, 0\rangle$) state to the acceptor state $|A, 0\rangle$. For the model system considered here, the energy of the photon-dressed acceptor state $|A, n\rangle$ (for $n \geq 1$) are far detuned from the rest of the polariton eigenspectrum, thus the electron transfer rate constant to these acceptor states are negligible in our model study, allowing us to focus on $|A, 0\rangle$ as the final state. This acceptor state has the energy $E_A = \langle A, 0|\hat{H}|A, 0\rangle$ with the following expression

$$E_{A,0} = \frac{1}{2} m_s \omega_s^2 (R_s - R_A^0)^2 + U_A + \frac{\hbar\omega_c}{2} \tag{38}$$

For the model considered here, the photon-dressed state $|G, 1\rangle$ has the same minimum as the $|D, 0\rangle$ state (because $R_G^0 = R_D^0$), producing the polariton state $|\pm, 0\rangle$ with the same potential energy minimum. The initial photoexcitation from the $|G, 0\rangle$ state to the $|\pm, 0\rangle$ state will lead to an *equilibrium* nuclear initial condition for the photoinduced system.

Assuming the equilibrium and quasi-classical nuclear initial conditions upon photoexcitation, we can use the Marcus Theory to describe the charge transfer rate between $|\pm, 0\rangle$ state to the $|A, 0\rangle$ state. The polariton-mediated electron transfer (PMET) rate constant is expressed as

$$k_c^{\pm} = \frac{|V_c^{\pm}|^2}{\hbar} \sqrt{\frac{\pi\beta}{\lambda}} \exp\left[-\beta \frac{(\Delta G_c^{\pm} + \lambda)^2}{4\lambda}\right] \tag{39}$$

where $\Delta G_c^{\pm}$ is the polariton-mediated driving force between the $|A, 0\rangle$ state (eq 38) and the $|\pm, 0\rangle$ state

$$\Delta G_c^{\pm} = E_{A,0}(R_A^0) - E_{\pm,0}(R_D^0) \tag{40}$$

and $V_c^{\pm}$ is the polariton-mediated coupling

$$V_c^{\pm} = \langle A, 0|\hat{H}_e|\pm, 0\rangle \tag{41}$$

Because the acceptor state does not carry any transition dipole, the matter-cavity coupling Hamiltonian $\hat{H}_{enp}$ (eq 16) does not provide any coupling between polariton states and the $|A, 0\rangle$ state. This is why polariton-mediated effective coupling $V_c^{\pm}$ only comes from the electronic Hamiltonian operator $\hat{H}_e$ (defined in eq 4).

By using eq 40 to describe PMET processes, we have not considered the photon decay in the cavity (10−50 ps in a photonic crystal cavity[127,128] and 10 ps in metal nanoparticle cavity arrays[129]), nonradiative decay of the excitation of matter (1−10 ns for NCs[127,128]), or the phonon-assisted upper to lower polariton population transfer.[127,130−132] The former two decay channels are slower than most of the PMET rate we considered here, thus we have ignored these two channels. Future studies will use direct PLDM quantum dynamics simulations to incorporate the photon leaking channel through either phenomenological modeling[133,134] or with the photon bath that couples to the cavity mode.[135] The upper to lower polariton transfer process can be assisted by the presence of phonon.[127,130,131] The upper and the lower polariton states (which are the eigenstates of $\hat{H}_{pl}$) are coupled to each other through the nuclear kinetic energy operator, and more explicitly, the nonadiabatic coupling $\langle -, 0|\nabla|+, 0\rangle$, where $\nabla \equiv \partial/\partial R_s$ is the nuclear gradient operator, as well as the second-derivative coupling. With the simple JC model Hamiltonian, it can be shown that[75] the derivative coupling is $\langle -, 0|\nabla|+, 0\rangle = (1 - \chi)/4g_c \cdot \nabla[E_D(R_s) - E_g(R_s)] - (\chi/\Delta\omega_c) \cdot \nabla g_c(R_s)$, where $\chi = \Delta\omega_c^2/(4g_c^2 + \Delta\omega_c^2)$. Thus, the phonon can couple the upper and lower polariton surfaces by potential curvature offset between the ground and excited electronic states (through $\nabla[E_D(R_s) - E_G(R_s)]$), as well as by the nuclear dependence of the light−matter interaction (through the $\nabla g_c(R_s)$ term). In our model, we assume that both $\nabla[E_D(R_s) - E_g(R_s)]$ and $\nabla g_c(R_s)$ equals to 0 (because we assume that the $|G\rangle$ and $|D\rangle$ state have the same curvature and a zero Huang−Rhys factor) leading to no

https://dx.doi.org/10.1021/acs.jpcb.0c03227
J. Phys. Chem. B XXXX, XXX, XXX−XXX

coupling between the upper and lower polariton states (under the RWA). In a real system, of course, the Huang−Rhys factor is not exactly zero, and future investigations will explicitly explore the phonon-assisted polariton population transfer during PMET. Nevertheless, existing experimental studies have suggested that the lifetime of the upper polariton can be as long as 20−60 ps under the resonance condition (at a relatively low temperature below 30 K),[127,128] much longer than the typical upper polariton lifetime for organic molecules coupled to the cavity[60,136] which is typically in a range of 50−150 fs.

On the basis of various levels of theoretical descriptions of the polariton eigenspectrum (as summarized in Table 2), we provide the detailed expressions of the polariton-mediated driving force and electronic coupling. We note that other similar expressions of PMET rate have been recently developed to investigate polariton-mediated electron transfer reaction.[77,78,137] Differently from these previous works, here, we explicitly consider the effects of the CRT and the DSE, both of which play an important role to correctly describe the polariton eigenenergy and hence, PMET rate constant in the ultrastrong coupling regime.

We emphasize that for the charge transfer model systems studied in this work, even the simplest Marcus theory is adequate to provide accurate rate constant, because of the weak donor−acceptor electronic coupling, quasi-classical behavior of R_s, and short memory-time for the bath modes. This is corroborated by the numerical results from our path-integral quantum dynamics simulations, which does not have these limitations in Marcus theory and can provide accurate charge transfer rate constant.[109] Hence, we take advantage of the conceptually simple Marcus theory to investigate the influence of the light−matter coupling on charge transfer kinetics. The above-mentioned limitations, however, can be conveniently addressed by using more accurate and advanced ET theories. The same analyses we have done in this work can be easily generalized and incorporated into those alternative ET rate theories to describe PMET processes. These recent theories and approaches are briefly outlined in the Supporting Information.

Rotating Wave Approximation. Assuming the RWA, the cavity-mediated driving force is

$$\begin{aligned}\Delta G_c^{\pm} &= E_{A,0}(R_A^0) - E_{\pm,0}^{(0)}(R_D^0)\\ &= \Delta G - \frac{1}{2}[\hbar\xi + \hbar\Delta\omega_c] \mp \frac{1}{2}\hbar\Omega_R,\end{aligned} \tag{42}$$

where we have used the results in eq 31 and eq 38. One can see that the DSE explicitly contribute to the PMET driving force. This is because that the transition dipoles $\boldsymbol{\mu}_{GD} = \boldsymbol{\mu}_0$ and $\boldsymbol{\mu}_{GA} = 0$ are different, leading to a finite difference of DSE associated with different states.

Under the RWA, the cavity-mediated electronic couplings between $|\pm, 0\rangle$ and $|A, 0\rangle$ states are

$$\begin{aligned}V_c^{+} &= \langle A, 0|\hat{H}_e|+, 0\rangle\\ &= \langle A, 0|\hat{H}_e[\sin\theta_c(0)|D, 0\rangle + \cos\theta_c(0)|G, 1\rangle]\\ &= \sin\theta_c(0)\cdot V_{DA},\\ V_c^{-} &= \langle A, 0|\hat{H}_e|-, 0\rangle\\ &= \langle A, 0|\hat{H}_e[\cos\theta_c(0)|D, 0\rangle - \sin\theta_c(0)|G, 1\rangle]\\ &= \cos\theta_c(0)\cdot V_{DA}.\end{aligned} \tag{43}$$

Here, we have used the fact that $\langle A, 0|\hat{H}_e|D, 0\rangle = \langle A|\hat{H}_e|D\rangle\langle 0|0\rangle = V_{DA}$ and $\langle A, 0|\hat{H}_e|G, 1\rangle = \langle A|\hat{H}_e|G\rangle\langle 0|1\rangle = 0$ (because $\langle 0|1\rangle = 0$, and we also assume $\langle A|\hat{H}_e|G\rangle = 0$ in our model). The mixing angle $\theta_c(n)$ is given in eq 28 (with $n = 0$ case).

Under the RWA-level description, the cavity QED process can mediate the charge transfer reaction by modifying the driving force $\Delta G_c^{\pm}$ (eq 42) and the effective electronic coupling $V_c^{\pm}$ (eq 43). This suggests that the ET dynamics can be mediated by changing the photon frequency ω_c (thus changing the detuning $\Delta\omega_c$ in $\Delta G_c^{\pm}$ and the mixing angle θ_c in $V_c^{\pm}$), as well as the light−matter coupling strength $\hbar g_c$ (thus changing the Rabi splitting Ω_c and dipole self-energy $\hbar\xi/2$ in $\Delta G_c^{\pm}$). Thus, coupling molecules to a cavity opens up new possibilities to control ET kinetics by using fundamental properties of quantum light−matter interactions.

Because that the mixing angle appears as $\sin\theta_c$ or $\cos\theta_c$ in $V_c^{\pm}$ (eq 43), the mixing among various photon-dressed states always decrease the electronic coupling (since $|\cos\theta_c| \le 1$ and $|\sin\theta_c| \le 1$). This is due to the fact that only $|D\rangle$ state is electronically coupled to the $|A\rangle$ state, whereas $|G\rangle$ does not; thus, mixing $|G, 1\rangle$ with $|D, 0\rangle$ effectively reduces the electronic coupling between the $|\pm, 0\rangle$ and $|A, 0\rangle$ state. This effect alone will reduce the ET rate due to the quadratic dependence of the $V_c^{\pm}$ in $k_c^{\pm}$ (eq 39). On the other hand, forming polaritons significantly change the driving force $\Delta G_c^{\pm}$ (eq 42), which exponentially impacts the PMET rate, enhancing or suppressing it depending on the sign of $\Delta G_c^{\pm} + \lambda$, (i.e., the Marcus turnover). The competition between the effect of $V_c^{\pm}$ and $\Delta G_c^{\pm} + \lambda$ provides exciting opportunities to alter the fundamental charge transfer kinetics. In this sense, the PMET process is akin to the proton-coupled electron transfer reaction (PCET), whereas in PCET, the presence of quantized vibrational levels of the transferring proton mediates both the effective vibronic couplings as well as the effective state-to-state driving force.[17,18]

By setting $\xi = 0$, the RWA Hamiltonian $\hat{H}_{pl}^{(0)}$ reduces to the JC Hamiltonian $\hat{H}_{JC}$ (eq 25) that ignores the DSE. The polariton-mediated driving force in eq 42 becomes the corresponding driving force in the JC model $\Delta G_{JC}^{\pm} = \Delta G - \hbar\Delta\omega_c/2 \mp \hbar\Omega_R/2$, whereas the polariton-mediated electronic coupling in eq 43 remains unchanged.

Perturbative Treatment. Explicitly considering the counter-rotating wave terms $\hat{H}_{pl}^{(1)}$ through the perturbation theory, and include the dipole self-energy, the polariton-mediated driving force is

$$\begin{aligned}\Delta G_c^{\pm} &= E_{A,0}(R_A^0) - (E_{\pm,0}^{(0)}(R_D^0) + E_{\pm,0}^{(2)}(R_D^0)),\\ &= \Delta G - \frac{1}{2}[\hbar\xi + \hbar\Delta\omega_c] \mp \frac{1}{2}\hbar\Omega_R - E_{\pm,0}^{(2)}(R_D^0),\end{aligned} \tag{44}$$

with $E_{\pm,0}^{(0)}$ and $E_{\pm,0}^{(2)}$ expressed in eq 31 and eq 34, respectively.

Furthermore, the first-order correction to the polaritonic states $|\pm, 0\rangle^{(1)}$ only introduces additional contributions from $|\pm, 2\rangle$, as suggested in eq 35. Thus, the $|\pm, 0\rangle^{(1)}$ does not couple to $|A, 0\rangle$ state due to the different number of photons. As a result, the polariton-mediated electronic coupling remains unchanged

$$\begin{aligned}V_c^{\pm} &= \langle A, 0|\hat{H}_e[|\pm, 0\rangle + |\pm, 0\rangle^{(1)}]\\ &= \langle A, 0|\hat{H}_e[|\pm, 0\rangle + c_+|+, 2\rangle + c_-|-, 2\rangle]\\ &= \langle A, 0|\hat{H}_e|\pm, 0\rangle.\end{aligned} \tag{45}$$

https://dx.doi.org/10.1021/acs.jpcb.0c03227
J. Phys. Chem. B XXXX, XXX, XXX−XXX

Note that the $|\pm, 2\rangle$ states do couple to the $|A, 2\rangle$ state. However, the energy of the $|A, 2\rangle$ state ($2\hbar\omega_c = 6$ eV higher than the $|A, 0\rangle$ state) is off-resonance with the rest of the states, and as a result, it does not contribute to the overall ET rate in the range of parameters considered here.

Exact Polariton Eigenstates. Consider the exact polariton eigenspectrum, the polariton-mediated driving force is expressed as

$$\Delta G_c^{\pm} = E_{A,0}(R_A^0) - E_{\pm,0}^{ex}(R_D^0) \tag{46}$$

where $E_{\pm,0}^{ex}$ (eq 37) is the exact eigenstate of $\hat{H}_{pl}$. The exact polariton eigenvector $|\pm, n\rangle^{(ex)}$ can be obtained by using extended coherent state approach,[85] or a large set of electronic-photonic basis $\{|\alpha, n\rangle\}$. Using the exact eigenvector we can compute the electronic coupling $V_c^{\pm} = \langle A, 0|\hat{H}_e|\pm, n\rangle^{(ex)}$. In this work, we have used a large set of photonic basis ($n = 10-15$) to converge these low-lying eigenstates, and we find the PMET rate constant based on the perturbative polariton eigenspectrum to agree well with the PMET rate constant with the exact solution.

Quantum Dynamics Simulations. To simulate polariton quantum dynamics, we extend the utility of dynamics approaches that were originally developed for molecular systems to describe the nonadiabatic transitions among polariton states, i.e., the electron-photon hybridized states. In particular, we apply the partial linearized density matrix (PLDM) path-integral approach[138] to propagate the quantum dynamics of the molecule−cavity hybrid system. PLDM is an approximate real-time path-integral method that has been successfully applied to investigate various nonadiabatic processes,[139−142] including excitation energy transfer[143] and charge transfer[109] across a broad range of coupling strength. A brief summary of this approach, together with the numerical details of the simulations are provided in the Supporting Information. Note that the direct quantum dynamics simulation does not assume any *a priori* assumptions of the coupling strength for $\hbar g_c$ or V_{DA}.

Here, we compute the time-dependent reduced density matrix of the light−matter hybrid system

$$\rho_{ij}(t) = \mathrm{Tr}_{\mathbf{R}}[\hat{\rho}(0)e^{i\hat{H}t/\hbar}|i\rangle\langle j|e^{-i\hat{H}t/\hbar}] \tag{47}$$

where, $\hat{H}$ is the total Hamiltonian (eq 2), $\mathrm{Tr}_{\mathbf{R}}$ represents the trace over the nuclear DOF, and $\hat{\rho}(0)$ represents the initial total density operator of the molecule−cavity hybrid system, and $\{|i\rangle, |j\rangle\} \in \{|\alpha, n\rangle\}$. In general, the charge transfer rate constant can be obtained by using the flux-side correlation function formalism $k = Q_r^{-1}\lim_{t\to t_p}\mathrm{Tr}_{\mathbf{R}}[\hat{\rho}\hat{F}e^{i\hat{H}t/\hbar}\hat{h}e^{-i\hat{H}t/\hbar}]$, where the side operator $\hat{h} = \sum_n|A, n\rangle\langle A, n|$ represents the dividing surface distinguishing reactant and product (where n is the number of the photon in the cavity), $\hat{F} = i/\hbar[\hat{H}, \hat{h}]$ is the flux operator, t_p is the plateau time of the correlation function, $\hat{\rho} = e^{-\beta\hat{H}}$ is the thermal density operator, and $Q_r = \mathrm{Tr}\,[\hat{\rho}\hat{h}]$ is the reactant partition function. PLDM has shown to provide accurate flux-side correlation function and predict an accurate rate constant across a wide range of parameters.[109,143] In this work, on the other hand, we obtain the rate by fitting[144,145] the population dynamics computed from PLDM (eq 47), with the details provided in the Supporting Information.

RESULTS AND DISCUSSIONS

In this section, we present the PMET rate obtained from both the analytic rate expression from eq 39 as well as from direct quantum dynamics simulations. For the analytic rate with the PF Hamiltonian, the polariton eigenspectrum is obtained with the perturbation theory and the polariton-mediated driving force and coupling are calculated based upon eq 44 and eq 45, respectively; for the analytic rate with the JC Hamiltonian, these quantities are calculated based upon eqs 42 and 43.

Figure 3 demonstrates the influence of the quantum light−matter interaction on the charge transfer rate constant at various

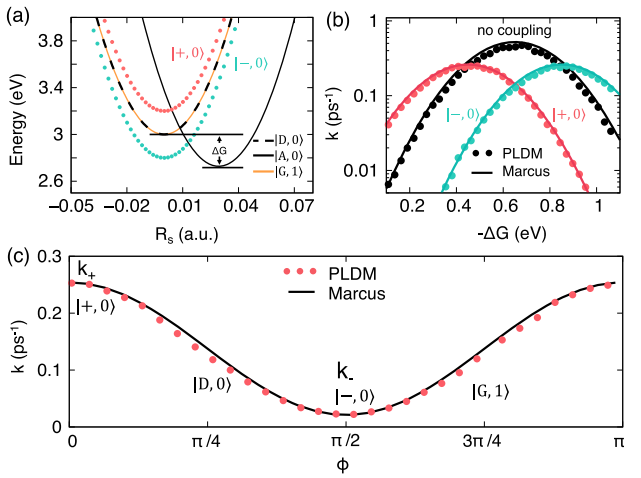

Figure 3. Modifying electron transfer rate through quantum light−matter interactions. (a) Potential energy surfaces of $|A, 0\rangle$ (solid black), $|D, 0\rangle$ (dashed black), and $|G, 1\rangle$ (yellow solid line) states and the polaritonic states $|+, 0\rangle$ (dotted red line) and $|-, 0\rangle$ (dotted green). (b) Electron transfer rate constant from $|+, 0\rangle$ (red) or $|-, 0\rangle$ (green) to the $|A, 0\rangle$ state when the NC−molecule is coupled with the cavity at a light−matter coupling strength $\hbar g_c = 0.2$ eV, compared to the electron transfer rate constant (black) in the bare NC−molecule system from the $|D\rangle$ state to the $|A\rangle$ state. The rate is presented as a function of the electronic driving force ΔG, obtained from both the PLDM quantum dynamics simulations (dotted) and with analytic rate expression (solid line). (c) Charge transfer rate as a function of ϕ under the initial condition $|\psi_0\rangle = \cos\phi|+, 0\rangle + \sin\phi|-,0\rangle$ at $\hbar g_c = 0.2$ eV and $\Delta G = -0.45$ eV.

electronic driving forces ΔG. The light−matter coupling strength is set to be $\hbar g_c = 0.2$ eV, the frequency of the cavity is $\hbar\omega_c = 3.0$ eV, and the detuning is set to be $\hbar\Delta\omega_c = 0$. In this case, $\frac{g_c}{\omega_c} < 0.1$; thus, DSE as well as the CR correction $E_{\pm,0}^{(2)}$ has negligible effects on the polariton energies and the PMET dynamics. The polariton-mediated driving force (given in eq 44) under this condition is $\Delta G_c^{\pm} = \Delta G - \frac{\hbar\xi}{2} \mp \hbar g_c - E_{\pm,0}^{(2)} \approx \Delta G \mp \hbar g_c$.

Figure 3a depicts the electron transfer model system, which includes an optically bright excited donor state $|D\rangle$ centered around $R_s = 0$, and a dark acceptor state $|A\rangle$ displaced by R_A^0 along the reaction coordinate R_s and shifted by the driving force ΔG. The ground state $|G\rangle$ of the molecular system is also centered around $R_s = 0$. The photon-dressed states considered here include $|G, 1\rangle$ which corresponds to the ground state of the molecule with 1 photon in the cavity (yellow solid line in Figure 3a), $|D, 0\rangle$ (black dashed line) and $|A, 0\rangle$ (black solid line) which are the donor and acceptor state with 0 photons in the cavity, respectively. The $|G, 1\rangle$ state is vertically shifted in energy with $\hbar\omega_c$ and in resonance with $|D, 0\rangle$. Through the light−matter coupling $\hbar g_c$, the optically bright $|D, 0\rangle$ state hybridizes with $|G, 1\rangle$ and generates $|+, 0\rangle \approx [|G, 1\rangle + |D, 0\rangle]/\sqrt{2}$ (red dotted line) and $|-, 0\rangle \approx [|G, 1\rangle - |D, 0\rangle]/\sqrt{2}$ (green dotted line) states that

https://dx.doi.org/10.1021/acs.jpcb.0c03227
J. Phys. Chem. B XXXX, XXX, XXX−XXX

are split by $\hbar\Omega_R$. These two polariton states (when RWA is valid for a small $\hbar g_c$) contains an equal superposition of the electronic excitation (of the NC−molecular system) and the photonic excitation (of the quantized mode in the cavity). In the coupled NC−molecule−cavity system, the optically bright states $|+, 0\rangle$ or $|-, 0\rangle$ can be populated through photoexcitation.[67] The acceptor state is coupled to the polariton state through $\langle \pm, 0|\hat{H}_{pl}|A, 0\rangle \approx V_{DA}/\sqrt{2}$, because $|+, 0\rangle$ and $|-, 0\rangle$ only contains $1/\sqrt{2}$ component of the donor electronic state which is directly coupled to the acceptor state through the electronic coupling. By photoexcitation of the hybrid system to its upper polariton state, we can tune the effective driving force of the PMET process by changing the light−matter coupling strength. This will have a significant impact on the charge transfer kinetics, as the rate constant is exponentially sensitive to the driving force (or reorganization energy). The overall PMET rate constant is influenced by a competition of the modified driving force and the reduced effective coupling.

Figure 3b presents the ET rate of the isolated NC−molecular system (black), and the polariton-mediated electron transfer rate when coupling the NC−molecule to the cavity, with the initial excitation to the $|+, 0\rangle$ state (red) or the $|-, 0\rangle$ state (green). The rate is presented as a function of the negative *electronic* driving force $-\Delta G$ (not to be confused with the polariton-mediated driving force $\Delta G_c^{\pm}$), obtained from both the analytic rate expression (solid line) and PLDM quantum dynamics simulations (dotted). For the bare NC−molecular system (black), the rate constant is described by the Marcus theory (eq 1), with a well-known parabolic shape in the logarithmic scale and a maximum of $\log k$ at $-\Delta G = \lambda = 0.65$ eV. When coupling the NC−molecule with the cavity under the resonance condition $\hbar\Delta\omega_c = 0$ (and with a negligible DSE and CRT), the light−matter interaction modifies the driving force as $\Delta G_c^{\pm} \approx \Delta G \mp \hbar g_c$, and the PMET rate constant maximizes at $-\Delta G_c^{\pm} = \lambda$, or equivalently, $-\Delta G \approx \lambda \mp \hbar g_c$ when exciting the system to the $|\pm, 0\rangle$ bright states. This effect is demonstrated in Figure 3b, with the corresponding maximum of the rate constant shifted by $-\hbar g_c$ for the $|+, 0\rangle$ state (red) and by $\hbar g_c$ for the $|-, 0\rangle$ (green) case, respectively. In addition, the electronic coupling between the bright polaritonic states $|\pm, 0\rangle$ and the acceptor state $|A, 0\rangle$ is $V_c^{\pm} = \cos\theta_c V_{DA} = V_{DA}/\sqrt{2}$ (see eq 43), which reduces the rate by 1/2 due to the quadratic dependence of the $V_c^{\pm}$ in the PMET rate constant (eq 39). Thus, the maximum PMET rate constant is only $^1/_2$ of the maximum rate constant in the bare NC−molecule system. On the other hand, for $\Delta G < \lambda - \hbar g_c$ or $\Delta G > \lambda + \hbar g_c$, the PMET rate can be suppressed or enhanced compared to the bare NC−molecule case.

Figure 3c demonstrates using initial conditions of the excitation to tune the electron transfer rate constant. Here, the initial photoexcitation is prepared as a superposition of $|+, 0\rangle$ and $|-, 0\rangle$ states as $|\psi_0\rangle = \cos\phi|+, 0\rangle + \sin\phi|-, 0\rangle$. The PMET rate constant as a function of ϕ at $\Delta G = -0.45$ eV and $\hbar g_c = 0.2$ eV is presented in Figure 3c. At $\phi = 0$ (or π) and $\pi/2$, the initial state $|\psi_0\rangle$ reduces to pure $|+, 0\rangle$ or $|-, 0\rangle$ states, respectively. Therefore, at these points, the PMET rate constants (denoted by k_+ and k_-, respectively) correspond to the values on the green and red curve at $\Delta G = -0.45$ eV in Figure 3b. The overall rate constant profile (solid black line in Figure 3c) can be computed as a weighted sum of k_+ and k_-, i.e., $k = \cos^2\phi k_+ + \sin^2\phi k_- = \cos^2\phi(k_+ - k_-) + k_-$, which matches the results from the PLDM simulations (red dots).

Figure 4 demonstrates using the light−matter coupling to tune the electron transfer rate constant. Here, the NC−molecule subsystem with $\Delta G = 0$ (symmetric charge transfer) is coupled to a cavity under the resonance condition $\hbar\Delta\omega_c = 0$.

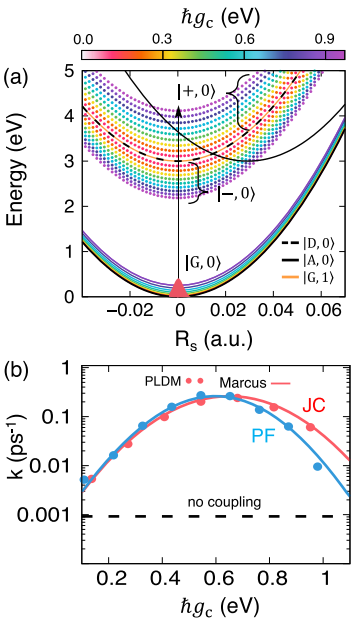

Figure 4. Control electron transfer rate by changing the coupling strength $\hbar g_c$ under the resonance condition $\Delta\omega_c = 0$ and a zero electronic driving force $\Delta G = 0$. (a) Polaritonic surfaces $|+, 0\rangle$ and $|-, 0\rangle$, color-coded according to the value of $\hbar g_c$ (top of the figure). (b) Electron transfer rate constant with the PF and the JC Hamiltonian, with the black dash line indicating the ET rate constant for the bare NC−molecule system.

Figure 4a presents the polaritonic surfaces of the $|+, 0\rangle$ and $|-, 0\rangle$ states, color coded according to the light−matter coupling strength $\hbar g_c$ (top panel of Figure 4a). With the perturbation theory (eq 44), the driving force between $|\pm, 0\rangle$ with $|A, 0\rangle$ is given by $\Delta G_c^{\pm} = \Delta G - \frac{\hbar\xi}{2} \mp \hbar g_c - E_{\pm,0}^{(2)}(R_D^0)$. At a smaller coupling strength $\hbar g_c < 0.25$ eV, the contribution from the DSE or CRT can be safely neglected, and as a result, the polariton energies for state $|+, 0\rangle$ and $|-, 0\rangle$ are shifted by an equal amount of $\hbar g_c$ with respect to the energy of $|G, 1\rangle$. At relatively large coupling strengths ($\hbar g_c > 0.25$ eV), the contributions from both the DSE and CRT become important, leading to an asymmetric splitting of the polariton energies as shown in Figure 4a (which can also be seen in Figure 2a). The overall positive contribution from the DSE and CRT terms enhances the splitting in E_+ and suppresses the splitting in EE_-.

Figure 4b presents the rate constants as a function of $\hbar g_c$, with the PF Hamiltonian that explicitly considers the DSE and the CRT (blue) and the JC Hamiltonian that ignores both (red). The ET rate constant in the bare NC−molecule system is indicated with the black dashed line. The JC rate constant curve is symmetric and exhibits an inversion at $-\Delta G_c^{+} = \lambda$, giving $\hbar\omega_c = \lambda = 0.65$ eV for this model system (under the condition $\Delta G = 0$ and $\hbar\Delta\omega_c = 0$). On the other hand, the PF rate constant curve is asymmetric due to the increasing positive contribution from the combined CRT and DSE terms. For $\hbar g_c < 0.65$ eV, the rate constant obtained from the PF Hamiltonian and the JC Hamiltonian agrees well with each other since the overall contribution from the CRT and the DSE is small. Increasing $\hbar g_c$ causes a large deviation of the JC rate from the exact rate obtained with the full PF Hamiltonian (up to 10 times differences in rate), demonstrating the importance of including

https://dx.doi.org/10.1021/acs.jpcb.0c03227
J. Phys. Chem. B XXXX, XXX, XXX−XXX

DSE and CRT in the USC regime. By tuning the light−matter coupling strength, one can enhance the rate constant by almost 2 orders of magnitude. We emphasize that the theory and the simulations do not consider other processes that are coupled to the ET reaction, such as the hole excitation in colloidal quantum dot[56] (which has been shown to prevent the presence of the Marcus inverted regime), the phonon-assisted upper to lower polariton population transfer,[127] and radiative and nonradiative decays of excitations.

Figure 5 presents various PMET regimes under the resonance condition ($\hbar\Delta\omega_c = 0$), with nonzero electronic driving forces,

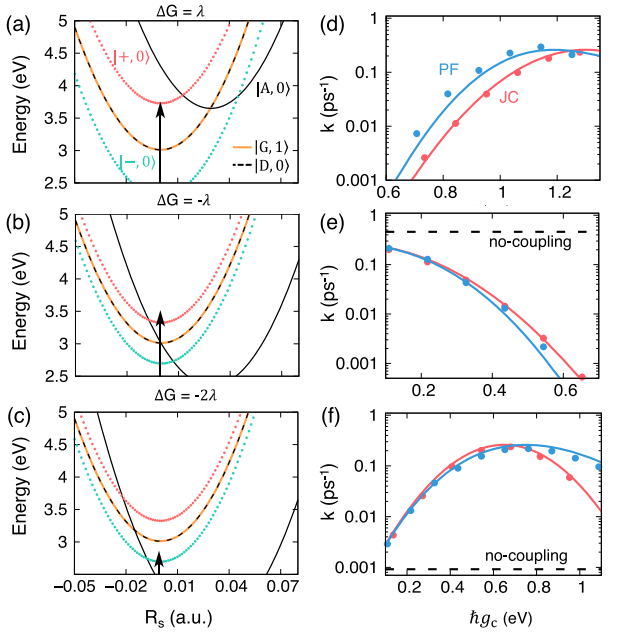

Figure 5. PMET rate with various electronic driving forces ΔG. Potentials for the polaritonic state $|+, 0\rangle$ (red dots), $|-, 0\rangle$ (green dots) and photon-dressed states $|D, 0\rangle$ (black dashed line), $|A, 0\rangle$ (black solid line), and $|G, 1\rangle$ state (yellow solid line). The electronic driving force is set to be (a) $\Delta G = \lambda$, (b) $\Delta G = -\lambda$ and (c) $\Delta G = 2\lambda$, with black arrow indicates the initial photoexcitation. The corresponding PMET rate is presented in panels d−f, respectively. The rate is obtained from both the analytic expression (solid) and the PLDM quantum dynamics simulation (dots), at the level of the PF Hamiltonian (blue) or the JC model (red).

including $\Delta G = \lambda$ (unfavorable uphill ET reaction), $\Delta G = -\lambda$ (activationless regime) and $\Delta G = -2\lambda$ (inverted regime). The potentials of these systems are presented in Figure 5a−c, and Figure 5d−f presents the corresponding electron transfer rate as a function of $\hbar g_c$ obtained from the PF and JC Hamiltonian through PMET expression (solid lines) and direct quantum dynamics simulations (dots).

Figure 5a presents the case when $\Delta G = \lambda$ (unfavorable uphill ET reaction), and the electron transfer rate constant for the NC−molecule system is off the scale in this figure ($k \approx 10^{-12}\text{ps}^{-1}$). The PMET rate constant is significantly enhanced when the NC−molecule subsystem is coupled to a cavity and is photoexcited to the $|+, 0\rangle$ state with a large coupling strength $\hbar g_c$, due to the enlarged cavity-mediated driving force ΔG_c^+. In Figure 5d, the electron transfer rate constant computed with the PF Hamiltonian increases until $\hbar g_c \sim 1.1$ eV and then shows an inversion when further increasing $\hbar g_c$. At such high $\hbar g_c$, the overall contributions of the DSE and the CRT are significant, and consequently, the rate constant computed with JC Hamiltonian deviates from those obtained from the full PF Hamiltonian. Numerical results obtained with quantum dynamics simulations agree well with the results obtained from the analytical rate expressions (eq 39). Thus, without the presence of the cavity (and the quantized mode of the EM field), there is no apparent charge transfer reaction due to the uphill driving force; by forming the light−matter hybridized polaritonic state, the driving force can be significantly changed to enable ET.

Figure 5b presents the results for a system with $\Delta G = -\lambda$, such that the NC−molecular system is in the activationless regime. By coupling to the cavity, the PMET rate constant is suppressed since both bright polariton states $|+, 0\rangle$ and $|-, 0\rangle$ are shifted away from the activationless region due to the light−matter interactions. The effective electronic coupling is also reduced by $V_c^{\pm} \approx V_{DA}/\sqrt{2}$, which further reduces the rate. The PMET rate between the $|+, 0\rangle$ and $|A, 0\rangle$ state as a function of $\hbar g_c$ is presented in Figure 5e. Photoexcitation to the $|-, 0\rangle$ state produces a qualitatively similar rate curve and is not shown here. For the range of $\hbar g_c$ represented here, the overall contributions of the DSE term and the CRT is smaller compared to the previous case.

Figure 5c presents the case when $\Delta G = -2\lambda$ for which the bare NC−molecular system lies in the Marcus inverted regime. Under this circumstance, the ET rate can be significantly enhanced by coupling the NC−molecule subsystem to a cavity when the hybrid system is photoexcited to the $|-, 0\rangle$ state. The driving force between the $|-, 0\rangle$ and $|A, 0\rangle$ state is $\Delta G_c^- = -2\lambda - \hbar\xi/2 + \hbar g_c + E_-^{(2)}$ for the PF Hamiltonian (eq 44). As shown in Figure 2a, for smaller values of the light−matter coupling strength ($\hbar g_c < 0.25$), the energy of the $|-, 0\rangle$ state shifts down linearly with increasing $\hbar g_c$. Ignoring the DSE and the CRT in the JC Hamiltonian leads only to a linear increase in $\Delta G_c^- = -2\lambda + \hbar g_c$ (with an increasing $\hbar g_c$), causing an inversion at $\hbar g_c = \lambda$ as the ΔG_c^- goes back to the normal regime from the originally inverted regime. On the other hand, at larger values of $\hbar g_c$, the overall contribution from the DSE and CRT shift the polariton energy in a different direction compared to the light−matter coupling strength $\hbar g_c$. As a result, the PMET rate curve for the PF Hamiltonian becomes noticeably wider with a peak shifted by ∼200 meV. Due to the presence of the DSE and CRT, the PMET rate curve based on the PF Hamiltonian (blue) in Figure 5f does not show a significant inversion of the rate constant in the range of $\hbar\omega_c$ presented here, whereas the PMET rate constant predicted by the JC model predicts an incorrect inversion.

So far, we have demonstrated that by changing the light−matter coupling strength under the resonance condition ($\hbar\Delta\omega_c = 0$), one can modify the PMET rate constant by mediating the effective driving force $\Delta G_c^{\pm}$ (which appears in the exponent of the PMET rate in eq 39), while keeping the polariton-mediated coupling $V_c^{\pm} \approx V_{DA}/\sqrt{2}$ a constant (due to the fact that under the resonance condition $|\pm, 0\rangle \approx [|G, 1\rangle + |D, 0\rangle]/\sqrt{2}$). On the other hand, when the cavity frequency $\hbar\omega_c$ is off-resonant with the electronic excitation $U_D - U_G$, both V_c and $\Delta G_c^{\pm}$ will be modified. Below, we show that we can take advantage of this effect to enhance the PMET rate constant.

In Figure 6, we explore the PMET processes under the off-resonance condition (when $\hbar\Delta\omega_c \neq 0$) while keeping the light−matter coupling as a constant. Because $\hbar g_c = \sqrt{\frac{\hbar\omega_c}{2\epsilon_0 \mathcal{V}}}\mu_0$, one could modify either ϵ_0 or $\mathcal{V}$ in the cavity to maintain a constant

https://dx.doi.org/10.1021/acs.jpcb.0c03227
J. Phys. Chem. B XXXX, XXX, XXX−XXX

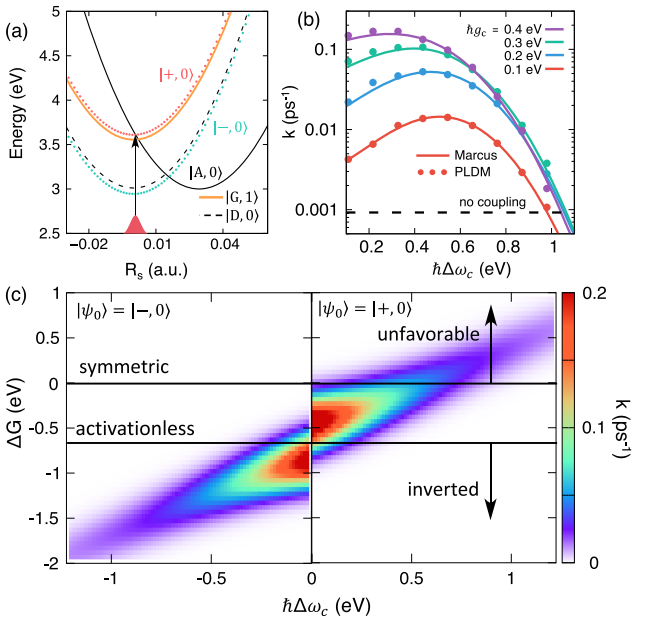

Figure 6. Controlling ET rate by changing the detuning $\hbar\Delta\omega_c$. (a) Potentials for light−matter hybrid states $|+, 0\rangle$ (red dots) and $|-, 0\rangle$ (green dots) at $\hbar g_c = 0.2$ eV and $\hbar\Delta\omega_c = 0.544$ eV. The photon dressed states are $|D, 0\rangle$ (black dashed line) and $|G, 1\rangle$ (solid orange line), and $|A, 0\rangle$ (solid black line). (b) Electron transfer rate constant from the $|+, 0\rangle$ state to the $|A, 0\rangle$ state as a function of $\hbar\Delta\omega_c$ at various $\hbar g_c$ computed from analytical rate expression (solid lines) as well as PLDM quantum dynamics simulations (dots). The black dashed line indicates the electron transfer rate in the bare NC−molecule system. (c) Enhancing electron transfer rate through the detuning frequency $\hbar\Delta\omega_c$ at various electronic driving force ΔG and a constant light matter coupling $\hbar g_c$ = 0.2 eV. The system is photoexcited to the $|+, 0\rangle$ state for positive detunings and to the $|-, 0\rangle$ state for negative detunings.

light−matter coupling strength while changing the frequency of the photon. Below, we demonstrate that the PMET rate constant can be significantly enhanced by coupling to an off-resonant cavity mode to tune the polariton-mediated driving force ΔG_c close to $-\lambda$ (i.e., the activationless regime), even when the polariton-mediated coupling $V_c^{\pm}$ (eq 43) becomes much smaller due to the relatively small contribution of the $|D, 0\rangle$ state in the $|+, 0\rangle$ state.

Figure 6a presents the potentials of the NC−molecule subsystem coupled to an off-resonant cavity. For this example, we set the electronic driving force $\Delta G = 0$ in the bare NC−molecule system for which the ET rate constant is small. We also set the cavity frequency to be $\hbar\omega_c = 3.45$ eV, for which the $|G, 1\rangle$ state (solid yellow line) is above the $|D, 0\rangle$ state (black dashed line) by $\hbar\Delta\omega_c = 0.45$ eV. The $|D, 0\rangle$ state hybridizes with the $|G, 1\rangle$ state through the coupling $\hbar g_c = 0.2$ eV, creating the $|+, 0\rangle$ (red dotted line) and $|-, 0\rangle$ (green dotted line) states which lie above the $|G, 1\rangle$ state and below the $|D, 0\rangle$ state, respectively. For electron transfer from the $|+, 0\rangle$ state, the exponent in the rate constant expression is maximized since $-\Delta G_c^{+} \approx \lambda$, corresponding to the activationless regime. Meanwhile, the polariton-mediated electronic coupling between the $|+, 0\rangle$ and $|A, 0\rangle$ states is $V_c^{+} = \sin\theta_c V_{DA}$, which is the original electronic coupling V_{DA} scaled down by $\sin\theta_c$. However, ΔG_c^{+} (which appears in the exponent of k_c^{+}) has a more pronounced effect on the PMET rate constant than the coupling V_c^{+} which appears as the prefactor of the rate expression (with a quadratic dependence). As a result, the overall rate constant is significantly enhanced by tuning the frequency of the photon while keeping the light−matter strength a constant.

Figure 6b presents the PMET rate constant as a function of the detuning frequency $\hbar\Delta\omega_c$ at several light−matter coupling strength $\hbar g_c$ for the model system presented in Figure 6a. The PMET rate constant is computed from the analytic rate constant expression in eq 39 (solid lines) or obtained from PLDM simulations (dots). The contribution of the DSE or the CRT (in the range of the coupling strength used here) is not significant and therefore, the rate computed from the JC model and PF model are essentially the same. Here,we only provide the results obtained from the PF Hamiltonian. The black dashed line represents the electron transfer rate between the donor and the acceptor states in the bare NC−molecule system. At a light−matter coupling strength of $\hbar g_c = 0.1$−0.3 eV, increasing in the detuning frequency $\hbar\Delta\omega_c$ leads to an enhancement of the electron transfer rate, until $\hbar\Delta\omega_c \approx 0.5$ eV. Further increasing $\hbar\Delta\omega_c$ causes the polariton-mediated driving force entering into the inverted regime $\left(\Delta G_c^{+} \approx -\frac{1}{2}(\hbar\xi + \hbar\Delta\omega_c) - \frac{1}{2}\sqrt{(\hbar\Delta\omega_c)^2 + 4(\hbar g_c)^2} < -\lambda\right)$, and with the additional decrease in V_c^{+}, the PMET rate constant decreases significantly, although it is still much larger than the ET rate in a bare NC−molecule system.

Figure 6c demonstrates the control of the ET rate constant with various range of electronic driving forces ΔG by tuning the photon frequency. The PMET rate is computed from eq 39 with the PF Hamiltonian by changing $\hbar\Delta\omega_c$ under a constant light−matter coupling $\hbar g_c = 0.2$ eV. For positive detuning frequencies, the system is photoexcited to the $|+, 0\rangle$ state, and for the negative detuning frequencies, it is photoexcited to $|-, 0\rangle$ state. Therefore, enhancing electron transfer through detuning could become a useful strategy when it is difficult to achieve a very strong light−matter coupling.

Note that although our theoretical investigations are closely related to previous studies,[77,78] they do provide new insights into PMET. In ref 77, the focus was placed on the polaron decoupling effect[146] through which the light−matter hybridization of the photon-dressed ground and the excited states reduce the effective Huang−Rhys factor (reorganization energy), thus enhancing the ET rate. In ref 78, the acceptor state is in resonance with the cavity. Depending on the choice of the photon frequency ω_c, the rate constant can be enhanced in the inverted regime and is largely unchanged in the normal regime.[78] In this work, we demonstrate a different control of the PMET rate through the hybridization of the $|G, 1\rangle$ and the $|D, 0\rangle$ states, leading to a significant enhancement or suppression of the rate constant.

Till now we have explored the PMET reaction with a weak electronic coupling $\beta V_{DA} \ll 1$. Next, we explore the situation when the electronic coupling between the donor and the acceptor state is large, i.e., $\beta V_{DA} \gg 1$. Because of this large electronic coupling (hence, the ET reaction lies in the adiabatic regime), the Marcus nonadiabatic ET theory is no longer adequate to provide an accurate rate. Thus, we will only present the results of direct numerical simulations from PLDM. Note that PLDM has proven to provide accurate rate constant for both the nonadiabatic and the adiabatic ET regimes.[109]

Figure 7a presents the polariton surface $E_L(R)$, which is the eigenenergy of the Hamiltonian $\hat{H}_{pl} = \hat{H}_e + \hat{H}_p + \hat{H}_{enp}$. Figure 7b presents the matrix elements of $\hat{H}_{pl}$ in the $|G, 1\rangle$ and $|D, 0\rangle$ and $|A, 0\rangle$ subspace. $|A, 0\rangle$ and $|G, 1\rangle$ do not directly couple to each other. But both them couple to $|D, 0\rangle$ and as a result they

https://dx.doi.org/10.1021/acs.jpcb.0c03227
J. Phys. Chem. B XXXX, XXX, XXX−XXX

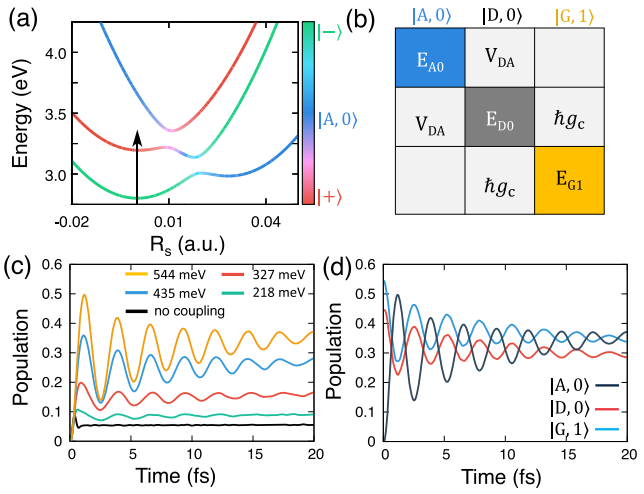

Figure 7. PMET dynamics with a strong electronic coupling V_{DA} = 100 meV. (a) Polaritonic potential with $\hbar g_c$ = 200 meV, color coded to represent the excitation charactor. (b) Matrix elements of the polariton Hamiltonian $\hat{H}_{pl}$ in the {|A, 0⟩, |D,0⟩, |G,1⟩} subspace. (c) Time-dependent acceptor population at different coupling strength $\hbar g_c$. (d) Population dynamics of |A, 0⟩, |D, 0⟩, and |G, 1⟩ at high light−matter coupling $\hbar g_c$ = 544 meV.

become effectively coupled to each other. Note that this polariton Hamiltonian is different than one defined in eq 17, where the projection operator $\hat{\mathcal{P}}$ is used to confine $\hat{H}_e$ within the {|D⟩, |G⟩} subspace. Here, we do not exclude the acceptor state, because it is strongly coupled to the donor state |D⟩ with V_{DA} = 100 meV. Because of the strong light−matter interaction between |G, 1⟩ and |D, 0⟩ state, the |A, 0⟩ state also couples to the |G, 1⟩ state indirectly through the |D, 0⟩ state. Thus, the presence of both the strong electronic coupling and the strong light−matter interactions induce large splittings between the eigensurfaces and resulting in a strong mixing between |D, 0⟩, |A, 0⟩, and |G, 1⟩ states.

Figure 7c provides the time-dependent population dynamics of the |A, 0⟩ state at various light−matter coupling strength $\hbar g_c$ obtained from the direct PLDM quantum dynamics simulation. The initial polaritonic wavepacket is prepared in the |+, 0⟩ state through a Franck−Condon excitation from the |G, 0⟩ state (indicated by a black arrow in Figure 7a). The presence of the strong electronic coupling V_{DA} causes a large polariton-mediated electronic coupling (eq 41) $V_c^+ \sim 70.7$ meV between |+, 0⟩ and |A, 0⟩ states, and induces oscillations in the |A, 0⟩ population. By increasing the light−matter coupling and hence the Rabi splitting (i.e., the gap between the |+, 0⟩ and |−, 0⟩ states), the energy gap between |+, 0⟩ and the |A, 0⟩ state is reduced, and the magnitude of oscillations become more prominent. This can be clearly seen at $\hbar g_c$ = 544 meV (yellow line) where the |+, 0⟩ state is in the activationless regime, and |A, 0⟩ and |+, 0⟩ states are strongly mixed due to the resonance condition. The magnitude of the population oscillation of the acceptor state also increases with the increasing light−matter coupling strength $\hbar g_c$.

Figure 7d presents the time-dependent population dynamics of the |G, 1⟩, |D, 0⟩, and |A, 0⟩ states at $\hbar g_c$ = 544 meV. The initial state |+, 0⟩ (with the solvent coordinate R_s in the Franck−Condon region) is a superposition of the |G, 1⟩ and |D, 0⟩ states. The presence of the strong coupling between |+, 0⟩ and |A, 0⟩ ($V_c^+ \sim 70.7$ meV) leads to oscillations in the population. The dissipative nuclear environment leads to a rapid decoherence process and the population plateaus after 50 fs. Through these direct simulations, we demonstrate that the strong light−matter interaction and electronic coupling can induce mixing between bright polariton state |+, 0⟩ and dark acceptor state |A, 0⟩. Thus, we envision that a strong electronic coupling between the donor and the acceptor state can be used to effectively couple quantized photonic states inside a cavity to the acceptor molecular state, even through the acceptor does not have a significant transition dipole and does not directly coupled to the cavity.

Note that the polariton-mediated charge transfer process presented in Figure 7 is in a different regime compared to the previous cases discussed in Figures 3−6. In the weak electronic coupling case (Figures 3−6), the charge transfer is mediated by fluctuations of the solvent, and the molecule−cavity interaction tailors the relative driving force and coupling. In the strong electronic coupling case (Figure 7), the charge transfer is induced by polariton-mediated population oscillations, which happens in a much faster time scale. One interesting possibility is to use the light−matter coupling to change the ET regime, from an originally adiabatic one, to the nonadiabatic regime. This is because that the PMET effective coupling $V_c^{\pm} = \langle A, 0 | \hat{H}_e | \pm, 0 \rangle$ is controlled by the donor component |D, 0⟩ in the polariton state |±, 0⟩ (see eq 43 and eq 45). For a resonance case presented in Figure 7, $|+, 0\rangle = (|D, 0\rangle + |G, 1\rangle)/\sqrt{2}$, hence effectively reduce the electronic coupling V_{DA} by $1/\sqrt{2}$. On the other hand, V_{DA} can be further decreased by changing the light−matter detuning, such that the electronic component is further reduced in the polariton states. Thus, by changing the light−matter detuning, one can switch the ET regimes from an originally adiabatic one to the nonadiabatic one, with the example provided in the Supporting Information. Coupling to the cavity provided a new strategy to switch the ET regimes by changing the light−matter detuning, as opposed to the existing approaches such as changing the donor−acceptor distance.

CONCLUSIONS

We investigate polariton-mediated charge transfer reaction between a bright donor state of a nanocrystal (NC) and a dark acceptor state associated with a molecule. By coupling the NC to an optical cavity, the electronically excited state |D, 0⟩ can hybridize with the photon-dressed ground state |G, 1⟩ through quantum light−matter interactions, forming polaritonic states. We demonstrate that both the effective driving force and the electronic coupling between these polaritonic states and the molecular acceptor state can be tuned by changing the photon frequency (hence the molecule−cavity detuning) and light−matter coupling strength, providing a new way to enhance or suppress the electron transfer dynamics. Through direct quantum dynamics simulations and analytic rate constant expressions, we demonstrate that forming polariton can (i) facilitate ET reactions even when the reaction is energetically uphill, (ii) enhance the rate in the inverted regime, (iii) or suppress the rate by the initial photoexcitation to the lower polariton state. Further, we demonstrate that the strong electronic coupling between the donor and the acceptor states can be used to effectively couple the quantized photonic state of a cavity to an optically dark acceptor molecular state. Our results clearly demonstrate several promising strategies of using the cavity polariton to mediate charge transfer reactions.

Our theoretical investigations start from the rigorous nonrelativistic QED Hamiltonian. We perform a systematic analysis of the accuracy for various commonly used model Hamiltonians in quantum optics, such as the Jaynes−Cummings

https://dx.doi.org/10.1021/acs.jpcb.0c03227
J. Phys. Chem. B XXXX, XXX, XXX−XXX

model that ignores both the counter-rotating terms (CRTs) and the dipole self-energy (DSE), and the Rabi model that ignores the DSE. We demonstrate that both the DSE and the CRT are required to be explicitly considered in order to accurately describe the polariton eigenspectrum and polariton-mediated charge transfer rate in the strong and ultrastrong coupling regimes.[88] With the perturbation theory, we show that for the lowest three polaritonic states, the Bloch−Siegert shift caused by the CRT is roughly half of the dipole self-energy, with an opposite sign, and including the DSE guarantees a bounded ground state.[95] The combined effects from the DSE and CRT enhances the splitting of the upper polariton branch and suppress the splitting of the lower polariton branch. The current work significantly complements the previous works in the direction of PMET,[77,78,137] where both the DSE and CRT terms are often ignored or overlooked. We provide analytic rate expression of PMET that explicitly considers their contributions, and demonstrate their importance through numerical examples. Our proposed PMET experiments and the PMET rate can also be potentially used as an effective way to measure the Bloch−Siegert shift and the dipole self-energy in a molecule−cavity hybrid system. We hope that our study helps to bridge photochemistry and quantum optics, and inspire future studies that take advantage of intrinsic QED effects to facilitate new chemical reactivities and transformations.

APPENDIX A: DERIVATION OF THE PAULI−FIERZ HAMILTONIAN

We provide a brief derivation of the commonly used Pauli−Fierz nonrelativistic Hamiltonian for light−matter interactions.[94,95] We begin by writing the electric field as $\mathbf{E}(\mathbf{r}) = \mathbf{E}_{\parallel}(\mathbf{r}) + \mathbf{E}_{\perp}(\mathbf{r})$, with its longitudinal part $\mathbf{E}_{\parallel}(\mathbf{r})$ that is curl free (irrotational) $\nabla\times \mathbf{E}_{\parallel}(\mathbf{r}) = 0$, and the transverse part that is divergence free (solenoidal) $\nabla\cdot\mathbf{E}_{\perp}(\mathbf{r}) = 0$. The magnetic field is purely transverse $\mathbf{B}(\mathbf{r}) = \mathbf{B}_{\perp}(\mathbf{r})$, because $\nabla\cdot\mathbf{B}(\mathbf{r}) = 0$.

By choosing the Coulomb gauge $\nabla\cdot\mathbf{A} = 0$ that makes the vector potential purely transverse, the Hamiltonian of N point charge particles (including both electrons and nuclei) can be written as follows

$$\hat{H} = \sum_{i}^{N} \frac{(\mathbf{p}_i - q_i\mathbf{A}_{\perp}(\mathbf{r}_i))^2}{2m_i} + \frac{\epsilon_0}{2}\int \mathrm{d}r^3\, \mathbf{E}_{\parallel}{}^2(\mathbf{r}) + \frac{\epsilon_0}{2}\int \mathrm{d}r^3\, [\mathbf{E}_{\perp}{}^2(\mathbf{r}) + c^2\mathbf{B}_{\perp}{}^2(\mathbf{r})], \tag{48}$$

where the sum includes *both* the nuclear and electronic DOFs, $\mathbf{r}_i$ and $\mathbf{p}_i$ are the position and momentum of the charged particle i, with the charge q_i and mass m_i. Furthermore, $\mathbf{A}_{\perp}(\mathbf{r})$, $\mathbf{E}_{\perp}(\mathbf{r})$ and $\mathbf{B}_{\perp}(\mathbf{r})$ are the transverse vector potential, electric field, and magnetic field, respectively. The energy associated with $\mathbf{E}_{\parallel}(\mathbf{r})$ (the second term in eq 48) is given by

$$\begin{aligned}&\frac{\epsilon_0}{2}\int \mathrm{d}r^3\, \mathbf{E}_{\parallel}{}^2(\mathbf{r})\\ &= \sum_i \frac{q_i{}^2}{2\epsilon_0(2\pi)^3}\int \frac{dk^3}{k^2} + \frac{1}{8\pi\epsilon_0}\sum_{i\neq j}\frac{q_iq_j}{|r_i - r_j|}\\ &= \sum_i \epsilon_i^{\infty} + V_{\mathrm{coul}}(\mathbf{r}) \to V_{\mathrm{coul}}(\mathbf{r}).\end{aligned} \tag{49}$$

Here, the first term $\sum_i \epsilon_i^{\infty}$ in the third line of eq 49 is a time-independent infinite quantity that is referred to as the self-energy (not to be confused with the dipole self-energy), which can be regarded as a shift of the zero-point energy[92] and is dropped in the last line of the above equation. In short, the coulomb potential $V_{\mathrm{coul}}(\mathbf{r})$ emerges from the longitudinal electric field.

The last term in eq 48 is the energy associated with the transverse fields $\mathbf{E}_{\perp}(\mathbf{r})$ and $\mathbf{B}_{\perp}(\mathbf{r})$. When charged particles are placed in a planar Fabry−Pérot (FB) microcavity, solutions of $\mathbf{A}_{\perp}(\mathbf{r})$, $\mathbf{E}_{\perp}(\mathbf{r})$, and $\mathbf{B}_{\perp}(\mathbf{r})$ that satisfy the boundary conditions are considered, and are quantized[91,92] as follows:

$$\mathbf{A}_{\perp}(\mathbf{r}) = \sum_j \frac{\hat{\epsilon}_j}{\omega_j}\sqrt{\frac{\hbar\omega_j}{2\epsilon_0\mathcal{V}}}\,(\hat{a}_j e^{i\mathbf{k}_j\cdot\mathbf{r}} + \hat{a}_j^{\dagger}e^{-i\mathbf{k}_j\cdot\mathbf{r}})$$

$$\mathbf{E}_{\perp}(\mathbf{r}) = i\sum_j \hat{\epsilon}_j\sqrt{\frac{\hbar\omega_j}{2\epsilon_0\mathcal{V}}}\,(\hat{a}_j e^{i\mathbf{k}_j\cdot\mathbf{r}} - \hat{a}_j^{\dagger}e^{-i\mathbf{k}_j\cdot\mathbf{r}})$$

$$\mathbf{B}_{\perp}(\mathbf{r}) = i\sum_j \frac{\mathbf{k}_j\times\hat{\epsilon}_j}{\omega_j}\sqrt{\frac{\hbar\omega_j}{2\epsilon_0\mathcal{V}}}\,(\hat{a}_j e^{i\mathbf{k}_j\cdot\mathbf{r}} - \hat{a}_j^{\dagger}e^{-i\mathbf{k}_j\cdot\mathbf{r}}).$$

Here, j is the index of the quantized radiational mode, $\hat{a}_j^{\dagger}$ and $\hat{a}_j$ are the creation and annihilation operators of photon, respectively, the frequency for mode j is $\omega_j = c\,|\mathbf{k}_j| = j\pi c/L$, where L is the distance between the mirrors, c is the speed of light, and $j \geq 1$ is an integer, $\mathbf{k}_j = |\mathbf{k}_j|\hat{\mathbf{k}}$ align in the direction of the unit vector $\hat{\mathbf{k}}$ that is perpendicular to the mirror surfaces, and $\hat{\epsilon}_j \perp \hat{k}$ is the polarization unit vector for $\mathbf{E}_{\perp}(\mathbf{r})$.

Using the above expressions, the energy of the transverse fields, i.e., the last term in eq 48 is quantized as follows

$$\frac{\epsilon_0}{2}\int_{\mathcal{V}} \mathrm{d}r^3\, [\mathbf{E}_{\perp}{}^2(\mathbf{r}) + c^2\mathbf{B}_{\perp}{}^2(\mathbf{r})] = \sum_j \left(\hat{a}_j^{\dagger}\hat{a}_j + \frac{1}{2}\right)\hbar\omega_j \tag{50}$$

where the spatial integral $\mathrm{d}r^3$ is done within the effective quantized volume $\mathcal{V}$ of the FB cavity.

Assuming that the dimension of the molecular system is much smaller than the length of the cavity, which is commonly referred to as the *long wavelength approximation*, the transverse fields can be treated as it is spatially uniform, i.e., $e^{i\mathbf{k}_j\cdot\mathbf{r}} \approx 1$, such that

$$\mathbf{A}_{\perp}(\mathbf{r}) \approx \mathbf{A}_{\perp} = \sum_j \frac{\hat{\epsilon}_j}{\omega_j}\sqrt{\frac{\hbar\omega_j}{2\epsilon_0\mathcal{V}}}\,(\hat{a}_j + \hat{a}_j^{\dagger}) \tag{51}$$

With the above approximation, the first term in eq 48 is expressed as

$$\sum_i^N \frac{(\mathbf{p}_i - q_i\mathbf{A}_{\perp}(\mathbf{r}_i))^2}{2m_i} \approx \sum_i^N \left[\frac{\mathbf{p}_i^2}{2m_i} - \frac{q_i}{m_i}\mathbf{p}_i\cdot\mathbf{A}_{\perp} + \frac{(q_i\mathbf{A}_{\perp})^2}{2m_i}\right] \tag{52}$$

Furthermore, we consider only a *single mode* of the radiation field along the $\hat{\epsilon}$ direction (which is commonly referred to as the single mode approximation in cavity QED), with the frequency $\omega_c = \pi c/L$ (c is the speed of the light, and ω_c represents the single mode frequency of the cavity), and the corresponding photonic creation and annihilation operators $\hat{a}^{\dagger}$ and $\hat{a}$. The single mode cavity-QED Hamiltonian under the long-wavelength limit in the Coulomb Gauge is then given as

https://dx.doi.org/10.1021/acs.jpcb.0c03227
J. Phys. Chem. B XXXX, XXX, XXX−XXX

$$\hat{H}_{\text{p·A}} = \sum_i^N \left[\frac{\mathbf{p}_i^2}{2m_i} - \frac{q_i \mathbf{p}_i \cdot \hat{\epsilon}}{\omega_c m_i} \sqrt{\frac{\hbar\omega_c}{2\varepsilon_0 \mathcal{V}}} (\hat{a} + \hat{a}^\dagger) + \frac{1}{2m_i} \left(\frac{q_i \hat{\epsilon}}{\omega_c} \sqrt{\frac{\hbar\omega_c}{2\varepsilon_0 \mathcal{V}}} (\hat{a} + \hat{a}^\dagger) \right)^2 \right] + V_{\text{coul}}(\mathbf{r}) + \left(\hat{a}^\dagger \hat{a} + \frac{1}{2} \right) \hbar\omega_c \tag{53}$$

The above Hamiltonian is referred to as the "p·A" Hamiltonian. The disadvantage of using the above Hamiltonian is that when assuming a two-level approximation in quantum optics (or a few-state approximation in a truncated Hilbert space) to describe the molecular system, the gauge invariance explicitly breaks down even in a moderate light−matter coupling strength, due to the breakdown of the locality of the potential energy operator.[147] On the other hand, the light−matter interaction Hamiltonian in the electric-dipole "d·E" form provide accurate results even when assuming a finite-level approximation of the molecule.[147,148] The difference between these two descriptions is rooted in the fundamental asymmetry between the position and the momentum operators. This can be easily seen by noticing $\mathrm{d}\hat{r}/\mathrm{dt} = \frac{1}{i\hbar}[\hat{r}, \hat{H}] = \hat{p}/m$, thus using the energy representation $\{|k\rangle\}$, one has $\langle k|[\hat{r},\hat{H}]|l\rangle = i\hbar m\langle k|\hat{p}|l\rangle$, i.e., $\langle k|\hat{r}|l\rangle \cdot (E_l - E_k) = i\hbar m \langle k|\hat{p}|l\rangle$. Even though $\langle k|\hat{r}|l\rangle$ only has an appreciable value for those states $|k\rangle$ and $|l\rangle$ that have small energy differences, the momentum operator in general, does not, because of the $(E_l - E_k)$ term that multiplies with the $\langle k|\hat{r}|l\rangle$. Thus, the large energy gaps in molecular system does not guarantee a small matrix element of the $\hat{p}$ operator,[148] hence a finite-level truncation in the "p·A" Hamiltonian often leads to large numerical errors. Note that such an asymmetry in $\hat{r}$ and $\hat{p}$ operators disappear for the electromagnetic mode or for a harmonically bound dipole, where momentum and position operators are interchangeable.[148] However, when the molecular potential is highly nonharmonic, the gauge invariance is explicitly broken under the finite-state approximation,[147] unless a complete basis for the molecule is used. Thus, it is often more convenient to use the dipole gauge when applying the finite-level approximation for the matter.[148]

To arrive at the convenient "d·E" form of the QED Hamiltonian,[91,92] we use the following Power−Zienau−Woolley (PZW) gauge transformation[91,94] under the dipole approximation

$$\hat{U}_{\text{pzw}} = \exp\left[\frac{i}{\hbar} \mathbf{A}_\perp \cdot \hat{\boldsymbol{\mu}}(\mathbf{r}) \right] \tag{54}$$

Here, $\hat{\boldsymbol{\mu}}(\mathbf{r}) = \sum_i q_i \mathbf{r}_i$ represents the total dipole operator of the molecular system (with contributions from both electrons and nuclei). This transformation is also commonly referred to as the length gauge,[94] electric-dipole gauge, or the Göppert-Mayer canonical transformation.[149]

Applying the above PZW gauge transformation on the "p·A" Hamiltonian (eq 53), one can obtain the light−matter interaction Hamiltonian in the "d·E" form (dipole−electric field interaction). This can be done by using the Baker−Hausdorff identity $e^{\hat{A}}\hat{B}e^{-\hat{A}} = \hat{B} + [\hat{A}, \hat{B}] + \frac{1}{2!}[\hat{A}, [\hat{A}, \hat{B}]] + \ldots$, and each individual term in $\hat{H}_{\text{p·A}}$ (eq 53) is transformed as follows

$$U_{\text{pzw}}^\dagger \left[\sum_i^N \frac{p_i^2}{2m_i} \right] U_{\text{pzw}} \rightarrow \sum_i^N \left[\frac{p_i^2}{2m_i} + \frac{q_i p_i \cdot \hat{\epsilon}}{\omega_c m_i} \sqrt{\frac{\hbar\omega_c}{2\varepsilon_0 \mathcal{V}}} (\hat{a} + \hat{a}^\dagger) + \frac{1}{2m_i} \left(q_i \frac{\hat{\epsilon}}{\omega_c} \sqrt{\frac{\hbar\omega_c}{2\varepsilon_0 \mathcal{V}}} (\hat{a} + \hat{a}^\dagger) \right)^2 \right] \tag{55}$$

$$U_{\text{pzw}}^\dagger \left[\sum_i^N -\frac{q_i p_i \cdot \hat{\epsilon}}{\omega_c m_i} \sqrt{\frac{\hbar\omega_c}{2\varepsilon_0 \mathcal{V}}} (\hat{a} + \hat{a}^\dagger) \right] U_{\text{pzw}} \rightarrow \sum_i^N \left[-\frac{q_i p_i \cdot \hat{\epsilon}}{\omega_c m_i} \sqrt{\frac{\hbar\omega_c}{2\varepsilon_0 \mathcal{V}}} (\hat{a} + \hat{a}^\dagger) - \frac{1}{m_i} \left(q_i \frac{\hat{\epsilon}}{\omega_c} \sqrt{\frac{\hbar\omega_c}{2\varepsilon_0 \mathcal{V}}} (\hat{a} + \hat{a}^\dagger) \right)^2 \right] \tag{56}$$

$$U_{\text{pzw}}^\dagger \left[\sum_i^N \frac{1}{2m_i} \left(q_i \frac{\hat{\epsilon}}{\omega_c} \sqrt{\frac{\hbar\omega_c}{2\varepsilon_0 \mathcal{V}}} (\hat{a} + \hat{a}^\dagger) \right)^2 \right] U_{\text{pzw}} \rightarrow \sum_i^N \frac{1}{2m_i} \left(q_i \frac{\hat{\epsilon}}{\omega_c} \sqrt{\frac{\hbar\omega_c}{2\varepsilon_0 \mathcal{V}}} (\hat{a} + \hat{a}^\dagger) \right)^2 \tag{57}$$

$$U_{\text{pzw}}^\dagger [V_{\text{coul}}(\mathbf{r})] U_{\text{pzw}} \rightarrow V_{\text{coul}}(\mathbf{r}) \tag{58}$$

$$U_{\text{pzw}}^\dagger \left[\left(\hat{a}^\dagger \hat{a} + \frac{1}{2} \right) \hbar\omega_c \right] U_{\text{pzw}} \rightarrow \left(\hat{a}^\dagger \hat{a} + \frac{1}{2} \right) \hbar\omega_c + i \sqrt{\frac{\hbar\omega_c}{2\varepsilon_0 \mathcal{V}}} \hat{\epsilon} \cdot \hat{\mu}(\mathbf{r}) (\hat{a}^\dagger - \hat{a}) + \frac{1}{\hbar\omega_c} \left(\sqrt{\frac{\hbar\omega_c}{2\varepsilon_0 \mathcal{V}}} \hat{\epsilon} \cdot \hat{\mu}(\mathbf{r}) \right)^2 \tag{59}$$

Note that the dipole self-energy arises from the PZW transform of the $(\hat{a}^\dagger \hat{a} + (^1/_2))\hbar\omega_c$ term in eq 59, and is not equivalent to the A^2 term in eq 57. These results can also be found in recent literature.[78,94]

Using the above results, the PZW transformation of the $\hat{H}_{\text{p·A}}$ Hamiltonian (eq 53) becomes

$$\hat{H}_{\text{d·E}} = U_{\text{pzw}}^\dagger \hat{H}_{\text{p·A}} U_{\text{pzw}} = \sum_i^N \frac{p_i^2}{2m_i} + V_{\text{coul}}(\mathbf{r}) + \left(\hat{a}^\dagger \hat{a} + \frac{1}{2} \right) \hbar\omega_c + i \sqrt{\frac{\hbar\omega_c}{2\varepsilon_0 \mathcal{V}}} \hat{\epsilon} \cdot \hat{\boldsymbol{\mu}}(\mathbf{r}) (\hat{a}^\dagger - \hat{a}) + \frac{1}{\hbar\omega_c} \left(\sqrt{\frac{\hbar\omega_c}{2\varepsilon_0 \mathcal{V}}} \hat{\epsilon} \cdot \hat{\boldsymbol{\mu}}(\mathbf{r}) \right)^2 \tag{60}$$

The above Hamiltonian, $\hat{H}_{\text{d·E}}$ is known as the "d·E" Hamiltonian, since the light matter coupling term involves the dipole operator and the transverse electric field, i.e., $i\sqrt{\frac{\hbar\omega_c}{2\epsilon_0 V_c}} \hat{\epsilon} \cdot \hat{\boldsymbol{\mu}}(\mathbf{r}) (\hat{a}^\dagger - \hat{a}) = -\hat{\boldsymbol{\mu}}(\mathbf{r}) \cdot \mathbf{E}_\perp$, where $\mathbf{E}_\perp = i\sqrt{\frac{\hbar\omega_c}{2\epsilon_0 V_c}} \hat{\epsilon} \cdot \hat{\boldsymbol{\mu}}(\mathbf{r}) (\hat{a} - \hat{a}^\dagger)$ is the transverse component of the E field associated with the single mode in the cavity under the long-wavelength limit. The "d·E" Hamiltonian can also be viewed as effectively using the Poincaré (multipolar) gauge,[91] where the vector potential under the Coulomb gauge upon PZW

https://dx.doi.org/10.1021/acs.jpcb.0c03227
J. Phys. Chem. B XXXX, XXX, XXX−XXX

transformation gives the new vector potential $\mathbf{A}'_{\parallel}(\mathbf{r}) = -\nabla\int_0^1 du\, \mathbf{r}\cdot\mathbf{A}_{\perp}(u\mathbf{r})$ and $\mathbf{A}'_{\perp}(\mathbf{r}) = \mathbf{A}_{\perp}(\mathbf{r})$. Note that in this new gauge, the vector potential is no longer purely transverse. This choice of the vector potential[91] makes $\mathbf{r}\cdot\mathbf{A}'(\mathbf{r}) = 0$. Thus, the Poincaré gauge enforces the vector potential to be perpendicular to $\mathbf{r}$ vector everywhere.

Furthermore, the above Hamiltonian with the complex light−matter coupling can be transformed into a new Hamiltonian with a real light−matter coupling, through a phase transformation with the following unitary operator

$$\hat{U}_\theta = \exp\left[i\frac{\pi}{2}\hat{a}^\dagger\hat{a}\right] \tag{61}$$

which gives $\hat{U}_\theta^\dagger\hat{a}\hat{U}_\theta \to i\hat{a}$ and $\hat{U}_\theta^T\hat{a}^\dagger\hat{U}_\theta \to -i\hat{a}^\dagger$. Applying this unitary transformation on $\hat{H}_{\text{d·E}}$ (and using the Baker−Hausdorff identity), we obtain the following Pauli−Fierz Hamiltonian

$$\hat{H}_{\text{PF}} = \hat{U}_\theta^\dagger\hat{H}_{\text{d·E}}\hat{U}_\theta = \sum_i^N \frac{p_i^2}{2m_i} + V_{\text{coul}}(\mathbf{r}) + \left(\hat{a}^\dagger\hat{a} + \frac{1}{2}\right)\hbar\omega_c + \sqrt{\frac{\hbar\omega_c}{2\epsilon_0 V_c}}\hat{\epsilon}\cdot\hat{\boldsymbol{\mu}}(\mathbf{r})(\hat{a}^\dagger + \hat{a}) + \frac{1}{\hbar\omega_c}\left(\sqrt{\frac{\hbar\omega_c}{2\epsilon_0 V_c}}\hat{\epsilon}\cdot\hat{\boldsymbol{\mu}}(\mathbf{r})\right)^2. \tag{62}$$

Here, $\sum_i^N \frac{p_i^2}{2m_i} + V_{\text{coul}}(\mathbf{r}) \equiv \hat{H}_{\text{en}}$ represents the molecular Hamiltonian, which includes all electrons and nuclei. $\hat{H}_{\text{PF}}$ is the Hamiltonian we used in eq 2.

■ ASSOCIATED CONTENT

Supporting Information

The Supporting Information is available free of charge at https://pubs.acs.org/doi/10.1021/acs.jpcb.0c03227.

Details of the derivation of the perturbative corrections, details of the partial linearized density matrix (PLDM) path−integral approach and the numerical details of the simulations, the fitting scheme for obtaining the PMET rate from the population dynamics, additional quantum dynamics simulations of PMET for polaron decoupling effect, additional results for weak light−matter interactions, and alternative theories for electron transfer (PDF)

Special Issue Paper

This paper was intended for the David N. Beratan Festschrift, published as the April 30, 2020, issue of *J. Phys. Chem. B* (Vol. 124, No. 17).

■ AUTHOR INFORMATION

Corresponding Authors

Arkajit Mandal − *Department of Chemistry, University of Rochester, Rochester, New York 14627, United States*; Phone: (585) 276-8358; Email: amandal4@ur.rochester.edu

Todd D. Krauss − *Department of Chemistry, University of Rochester, Rochester, New York 14627, United States*; orcid.org/0000-0002-4860-874X; Phone: (585) 275-5093; Email: krauss@chem.rochester.edu

Pengfei Huo − *Department of Chemistry, University of Rochester, Rochester, New York 14627, United States*; orcid.org/0000-0002-8639-9299; Phone: (585) 276-7793; Email: pengfei.huo@rochester.edu

Complete contact information is available at: https://pubs.acs.org/10.1021/acs.jpcb.0c03227

Notes

The authors declare no competing financial interest.

■ ACKNOWLEDGMENTS

This work was supported by the National Science Foundation "Enabling Quantum Leap in Chemistry" program under Grant Numbers CHE-1836546 and CHE-1836566. Computing resources were provided by the Center for Integrated Research Computing (CIRC) at the University of Rochester. P.H. acknowledges the support from his Cottrell Scholar award. A.M. appreciates the support from his Elon Huntington Hooker Fellowship and stimulating discussions with Wanghuai Zhou, Marwa Farag, and Tao Li. We appreciate valuable conversations with Profs. Nick Vamivakas, Joe Eberly, and Peter Milonni. We would also like to thank Prof. David Beratan for inspiring our work in the field of charge transfer and beyond.

■ REFERENCES

(1) Marcus, R. A. On the Theory of Oxidation-Reduction Reactions Involving Electron Transfer. I. *J. Chem. Phys.* **1956**, *24*, 966−978.

(2) May, V.; Kühn, O. *Charge and Energy Transfer Dynamics in Molecular Systems*; John Wiley & Sons, Inc.: Hoboken, NJ, 2011.

(3) Nitzan, A. *Chemical Dynamics in Condensed Phases: Relaxation, Transfer and Reactions in Condensed Molecular Systems*; Oxford University Press: Oxford, U.K., 2006.

(4) Miller, J. R.; Calcaterra, L. T.; Closs, G. L. Intramolecular Long-Distance Electron Transfer in Radical Anions. The Effects of Free Energy and Solvent on the Reaction Rates. *J. Am. Chem. Soc.* **1984**, *106*, 3047−3049.

(5) Marcus, R.; Sutin, N. Electron Transfers in Chemistry and Biology. *Biochim. Biophys. Acta, Rev. Bioenerg.* **1985**, *811*, 265−322.

(6) Thomas, L.; Hicks, K. W. Kinetics of the Permanganate Ion-Potassium Octacyanomolybdate(IV) Reaction. *Inorg. Chem.* **1974**, *13*, 749−752.

(7) Weaver, M. J.; Yee, E. L. Activation Parameters for Homogeneous Outer-Sphere Electron-Transfer Reactions. Comparisons Between Self-Exchange and Cross Reactions Using Marcus' Theory. *Inorg. Chem.* **1980**, *19*, 1936−1945.

(8) Silverman, D. N. Marcus Rate Theory Applied to Enzymatic Proton Transfer. *Biochim. Biophys. Acta, Bioenerg.* **2000**, *1458*, 88−103.

(9) Mayer, J. M. Understanding Hydrogen Atom Transfer: From Bond Strengths to Marcus Theory. *Acc. Chem. Res.* **2011**, *44*, 36−46.

(10) Nitzan, A.; Jortner, J.; Rentzepis, P. M.; Porter, G. Intermediate Level Structure in Highly Excited Electronic States of Large Molecules. *Proc. R. Soc. London, Ser. A* **1972**, *327*, 367−391.

(11) Ulstrup, J.; Jortner, J. The Effect of Intramolecular Quantum Modes on Free Energy Relationships for Electron Transfer Reactions. *J. Chem. Phys.* **1975**, *63*, 4358−4368.

(12) Efrima, S.; Bixon, M. On the Role of Vibrational Excitation in Electron Transfer Reactions With Large Negative Free Energies. *Chem. Phys. Lett.* **1974**, *25*, 34−37.

(13) Jortner, J. Temperature Dependent Activation Energy for Electron Transfer Between Biological Molecules. *J. Chem. Phys.* **1976**, *64*, 4860−4867.

(14) Kestner, N. R.; Logan, J.; Jortner, J. Thermal Electron Transfer Reactions in Polar Solvents. *J. Phys. Chem.* **1974**, *78*, 2148−2166.

(15) Likhtenshtein, G. *Solar Energy Conversion*; John Wiley & Sons, Inc.: Hoboken, NJ, 2012.

(16) Migliore, A.; Polizzi, N. F.; Therien, M. J.; Beratan, D. N. Biochemistry and Theory of Proton-Coupled Electron Transfer. *Chem. Rev.* **2014**, *114*, 3381−3465.

(17) Hammes-Schiffer, S. Proton-Coupled Electron Transfer: Classification Scheme and Guide to Theoretical Methods. *Energy Environ. Sci.* **2012**, *5*, 7696−7703.

(18) Hammes-Schiffer, S.; Stuchebrukhov, A. A. Theory of Coupled Electron and Proton Transfer Reactions. *Chem. Rev.* **2010**, *110*, 6939−6960.
(19) Cukier, R. I.; Nocera, D. G. Proton-Coupled Electron Transfer. *Annu. Rev. Phys. Chem.* **1998**, *49*, 337−369.
(20) Cukier, R. I. Proton-Coupled Electron Transfer Reactions: Evaluation of Rate Constants. *J. Phys. Chem.* **1996**, *100*, 15428−15443.
(21) Cukier, R. I. A Theory that Connects Proton-Coupled Electron-Transfer and Hydrogen-Atom Transfer Reactions. *J. Phys. Chem. B* **2002**, *106*, 1746−1757.
(22) Borgis, D.; Hynes, J. T. Curve Crossing Formulation for Proton Transfer Reactions in Solution. *J. Phys. Chem.* **1996**, *100*, 1118−1128.
(23) Hammes-Schiffer, S.; Soudackov, A. V. Proton-Coupled Electron Transfer in Solution, Proteins, and Electrochemistry. *J. Phys. Chem. B* **2008**, *112*, 14108−14123.
(24) Soudackov, A.; Hammes-Schiffer, S. Derivation of Rate Expressions for Nonadiabatic Proton-Coupled Electron Transfer Reactions in Solution. *J. Chem. Phys.* **2000**, *113*, 2385−2396.
(25) Warren, J. J.; Tronic, T. A.; Mayer, J. M. Thermochemistry of Proton-Coupled Electron Transfer Reagents and its Implications. *Chem. Rev.* **2010**, *110*, 6961−7001.
(26) Davis, W. B.; Ratner, M. A.; Wasielewski, M. R. Conformational Gating of Long Distance Electron Transfer through Wire-like Bridges in Donor-Bridge-Acceptor Molecules. *J. Am. Chem. Soc.* **2001**, *123*, 7877−7886.
(27) Beratan, D. N.; Onuchic, J. N.; Hopfield, J. J. Electron Tunneling Through Covalent and Noncovalent Pathways in Proteins. *J. Chem. Phys.* **1987**, *86*, 4488−4498.
(28) Beratan, D. N.; Onuchic, J. N. Electron Tunneling Pathways in Proteins: Influences on the Transfer Rate. *Photosynth. Res.* **1989**, *22*, 173−186.
(29) Onuchic, J. N.; Beratan, D. N. A Predictive Theoretical Model for Electron Tunneling Pathways in Proteins. *J. Chem. Phys.* **1990**, *92*, 722−733.
(30) Troisi, A.; Nitzan, A.; Ratner, M. A. A Rate Constant Expression for Charge Transfer Through Fluctuating Bridges. *J. Chem. Phys.* **2003**, *119*, 5782−5788.
(31) Skourtis, S. S.; Waldeck, D. H.; Beratan, D. N. Fluctuations in Biological and Bioinspired Electron-Transfer Reactions. *Annu. Rev. Phys. Chem.* **2010**, *61*, 461−485.
(32) Troisi, A.; Nitzan, A.; Ratner, M. A. A Rate Constant Expression for Charge Transfer Through Fluctuating Bridges. *J. Chem. Phys.* **2003**, *119*, 5782−5788.
(33) Goychuk, I. A.; Petrov, E. G.; May, V. Bridge-Assisted Electron Transfer Driven by Dichotomically Fluctuating Tunneling Coupling. *J. Chem. Phys.* **1995**, *103*, 4937−4944.
(34) Beratan, D. N.; Skourtis, S.; Balabin, I. A.; Balaeff, A.; Keinan, S.; Venkatramani, R.; Xiao, D. Steering Electrons on Moving Pathways. *Acc. Chem. Res.* **2009**, *42*, 1669−1678.
(35) Prytkova, T. R.; Kurnikov, I. V.; Beratan, D. N. Coupling Coherence Distinguishes Structure Sensitivity in Protein Electron Transfer. *Science* **2007**, *315*, 622−625.
(36) Antony, J.; Medvedev, D. M.; Stuchebrukhov, A. A. Theoretical Study of Electron Transfer between the Photolyase Catalytic Cofactor FADH- and DNA Thymine Dimer. *J. Am. Chem. Soc.* **2000**, *122*, 1057−1065.
(37) Medvedev, E. S.; Stuchebrukhov, A. A. Inelastic Tunneling in Long-Distance Biological Electron Transfer Reactions. *J. Chem. Phys.* **1997**, *107*, 3821−3831.
(38) Daizadeh, I.; Medvedev, E. S.; Stuchebrukhov, A. A. Effect of Protein Dynamics on Biological Electron Transfer. *Proc. Natl. Acad. Sci. U. S. A.* **1997**, *94*, 3703−3708.
(39) Craven, G. T.; Nitzan, A. Electron Transfer Across a Thermal Gradient. *Proc. Natl. Acad. Sci. U. S. A.* **2016**, *113*, 9421−9429.
(40) Craven, G. T.; Nitzan, A. Electron Transfer at Thermally Heterogeneous Molecule-Metal Interfaces. *J. Chem. Phys.* **2017**, *146*, 092305.
(41) Craven, G. T.; Nitzan, A. Electrothermal Transistor Effect and Cyclic Electronic Currents in Multithermal Charge Transfer Networks. *Phys. Rev. Lett.* **2017**, *118*, 207201.
(42) Antoniou, P.; Ma, Z.; Zhang, P.; Beratan, D. N.; Skourtis, S. S. Vibrational Control of Electron-Transfer Reactions: A Feasibility Study for the Fast Coherent Transfer Regime. *Phys. Chem. Chem. Phys.* **2015**, *17*, 30854−30866.
(43) Ma, Z.; Antoniou, P.; Zhang, P.; Skourtis, S. S.; Beratan, D. N. A Nonequilibrium Molecular Dynamics Study of Infrared Perturbed Electron Transfer. *J. Chem. Theory Comput.* **2018**, *14*, 4818−4832.
(44) Rubtsov, I. V. State-Specific Electron Transfer: Shake It Off. *Nat. Chem.* **2015**, *7*, 683−684.
(45) Franco, I.; Shapiro, M.; Brumer, P. Robust Ultrafast Currents in Molecular Wires through Stark Shifts. *Phys. Rev. Lett.* **2007**, *99*, 126802.
(46) Schiffrin, A.; Paasch-Colberg, T.; Karpowicz, N.; Apalkov, V.; Gerster, D.; Mühlbrandt, S.; Korbman, M.; Reichert, J.; Schultze, M.; Holzner, S.; et al. Optical-Field-Induced Current in Dielectrics. *Nature* **2013**, *493*, 70−74.
(47) Garzón-Ramírez, A. J.; Franco, I. Stark Control of Electrons Across Interfaces. *Phys. Rev. B: Condens. Matter Mater. Phys.* **2018**, *98*, 121305.
(48) Skourtis, S. S.; Beratan, D. N.; Waldeck, D. H. Coherence in Electron Transfer Pathways. *Procedia Chem.* **2011**, *3*, 99−104.
(49) Lin, J.; Balamurugan, D.; Zhang, P.; Skourtis, S. S.; Beratan, D. N. Two-Electron Transfer Pathways. *J. Phys. Chem. B* **2015**, *119*, 7589−7597.
(50) Prytkova, T. R.; Beratan, D. N.; Skourtis, S. S. Photoselected Electron Transfer Pathways in DNA Photolyase. *Proc. Natl. Acad. Sci. U. S. A.* **2007**, *104*, 802−807.
(51) Goldsmith, R. H.; Wasielewski, M. R.; Ratner, M. A. Transfer in Multiply Bridged Donor-Acceptor Molecules: Dephasing and Quantum Coherence. *J. Phys. Chem. B* **2006**, *110*, 20258−20262.
(52) Zarea, M.; Powell, D.; Renaud, N.; Wasielewski, M. R.; Ratner, M. A. Decoherence and Quantum Interference in a Four-Site Model System: Mechanisms and Turnovers. *J. Phys. Chem. B* **2013**, *117*, 1010−1020.
(53) Renaud, N.; Powell, D.; Zarea, M.; Movaghar, B.; Wasielewski, M. R.; Ratner, M. A. Quantum Interferences and Electron Transfer in Photosystem I. *J. Phys. Chem. A* **2013**, *117*, 5899−5908.
(54) Yuly, J. L.; Lubner, C. E.; Zhang, P.; Beratan, D. N.; Peters, J. W. Electron Bifurcation: Progress and Grand Challenges. *Chem. Commun.* **2019**, *55*, 11823−11832.
(55) Zhang, P.; Yuly, J. L.; Lubner, C. E.; Mulder, D. W.; King, P. W.; Peters, O. W.; Beratan, D. N. Electron Bifurcation: Thermodynamics and Kinetics of Two-Electron Brokering in Biological Redox Chemistry. *Acc. Chem. Res.* **2017**, *50*, 2410−2417.
(56) Zhu, H.; Yang, Y.; Hyeon-Deuk, K.; Califano, M.; Song, N.; Wang, Y.; Zhang, W.; Prezhdo, O. V.; Lian, T. Auger-Assisted Electron Transfer from Photoexcited Semiconductor Quantum Dots. *Nano Lett.* **2014**, *14*, 1263−1269.
(57) Olshansky, J. H.; Balan, A. D.; Ding, T. X.; Fu, X.; Lee, Y. V.; Alivisatos, A. P. Temperature-Dependent Hole Transfer from Photoexcited Quantum Dots to Molecular Species: Evidence for Trap-Mediated Transfer. *ACS Nano* **2017**, *11*, 8346−8355.
(58) Olshansky, J. H.; Ding, T. X.; Lee, Y. V.; Leone, S. R.; Alivisatos, A. P. Hole Transfer from Photoexcited Quantum Dots: The Relationship between Driving Force and Rate. *J. Am. Chem. Soc.* **2015**, *137*, 15567−15575.
(59) Ding, T. X.; Olshansky, J. H.; Leone, S. R.; Alivisatos, A. P. Efficiency of Hole Transfer from Photoexcited Quantum Dots to Covalently Linked Molecular Species. *J. Am. Chem. Soc.* **2015**, *137*, 2021−2029.
(60) Hutchison, J. A.; Schwartz, T.; Genet, C.; Devaux, E.; Ebbesen, T. W. Modifying Chemical Landscapes by Coupling to Vacuum Fields. *Angew. Chem., Int. Ed.* **2012**, *51*, 1592−1596.
(61) Schwartz, T.; Hutchison, J. A.; Genet, C.; Ebbesen, T. W. Reversible Switching of Ultrastrong Light-Molecule Coupling. *Phys. Rev. Lett.* **2011**, *106*, 196405.

https://dx.doi.org/10.1021/acs.jpcb.0c03227
J. Phys. Chem. B XXXX, XXX, XXX−XXX

(62) Munkhbat, B.; Wersall, M.; Baranov, D. G.; Antosiewicz, T. J.; Shegai, T. Suppression of Photo-Oxidation of Organic Chromophores by Strong Coupling to Plasmonic Nanoantennas. *Sci. Adv.* **2018**, *4*, eaas9552.
(63) Stranius, K.; Hertzog, M.; Börjesson, K. Selective Manipulation of Electronically Excited States Through Strong Light-Matter Interactions. *Nat. Commun.* **2018**, *9*, 2273.
(64) Kowalewski, M.; Mukamel, S. Manipulating Molecules with Quantum Light. *Proc. Natl. Acad. Sci. U. S. A.* **2017**, *114*, 3278−3280.
(65) Feist, J.; Galego, J.; Garcia-Vidal, F. J. Polaritonic Chemistry with Organic Molecules. *ACS Photonics* **2018**, *5*, 205−216.
(66) Mandal, A.; Huo, P. Investigating New Reactivities Enabled by Polariton Photochemistry. *J. Phys. Chem. Lett.* **2019**, *10*, 5519−5529.
(67) Ebbesen, T. W. Hybrid Light-Matter States in a Molecular and Material Science Perspective. *Acc. Chem. Res.* **2016**, *49*, 2403−2412.
(68) Thomas, A.; Lethuillier-Karl, L.; Nagarajan, K.; Vergauwe, R.; George, J.; Chervy, T.; Shalabney, A.; Devaux, E.; Genet, C.; Moran, J.; Ebbesen, T. Tilting a Ground-State Reactivity Landscape by Vibrational Strong Coupling. *Science* **2019**, *363*, 615−619.
(69) Flick, J.; Ruggenthaler, M.; Appel, H.; Rubio, A. Atoms and Molecules in Cavities, from Weak to Strong Coupling in Quantum-Electrodynamics (QED) Chemistry. *Proc. Natl. Acad. Sci. U. S. A.* **2017**, *114*, 3026−3034.
(70) Ribeiro, R. F.; Martínez-Martínez, L. A.; Du, M.; Campos-Gonzalez-Angulo, J.; Yuen-Zhou, J. Polariton Chemistry: Controlling Molecular Dynamics With Optical Cavities. *Chem. Sci.* **2018**, *9*, 6325−6339.
(71) Galego, J.; Garcia-Vidal, F. J.; Feist, J. Suppressing Photochemical Reactions with Quantized Light Fields. *Nat. Commun.* **2016**, *7*, 13841EP.
(72) Galego, J.; Garcia-Vidal, F. J.; Feist, J. Many-Molecule Reaction Triggered by a Single Photon in Polaritonic Chemistry. *Phys. Rev. Lett.* **2017**, *119*, 136001.
(73) Galego, J.; Garcia-Vidal, F. J.; Feist, J. Cavity-Induced Modifications of Molecular Structure in the Strong-Coupling Regime. *Phys. Rev. X* **2015**, *5*, 041022.
(74) Kowalewski, M.; Bennett, K.; Mukamel, S. Cavity Femtochemistry: Manipulating Nonadiabatic Dynamics at Avoided Crossings. *J. Phys. Chem. Lett.* **2016**, *7*, 2050−2054.
(75) Kowalewski, M.; Bennett, K.; Mukamel, S. Non-Adiabatic Dynamics of Molecules in Optical Cavities. *J. Chem. Phys.* **2016**, *144*, 054309.
(76) Triana, J. F.; Peláez, D.; Sanz-Vicario, J. L. Entangled Photonic-Nuclear Molecular Dynamics of LiF in Quantum Optical Cavities. *J. Phys. Chem. A* **2018**, *122*, 2266−2278.
(77) Herrera, F.; Spano, F. C. Cavity-Controlled Chemistry in Molecular Ensembles. *Phys. Rev. Lett.* **2016**, *116*, 238301.
(78) Semenov, A.; Nitzan, A. Electron Transfer in Confined Electromagnetic Fields. *J. Chem. Phys.* **2019**, *150*, 174122.
(79) Schäfer, C.; Ruggenthaler, M.; Appel, H.; Rubio, A. Modification of Excitation and Charge Transfer in Cavity Quantum-Electrodynamical Chemistry. *Proc. Natl. Acad. Sci. U. S. A.* **2019**, *116*, 4883−4892.
(80) Sentef, M. A.; Ruggenthaler, M.; Rubio, A. Cavity Quantum-Electrodynamical Polaritonically Enhanced Electron-Phonon Coupling and Its Influence on Superconductivity. *Sci. Adv.* **2018**, *4*, eaau6969.
(81) Martinez-Martinez, L. A.; Du, M.; Ribeiro, R.; Kéna-Cohen, S.; Yuen-Zhou, J. Polariton-Assisted Singlet Fission in Acene Aggregates. *J. Phys. Chem. Lett.* **2018**, *9*, 1951−1957.
(82) Du, M.; Ribeiro, R. F.; Yuen-Zhou, J. Remote Control of Chemistry in Optical Cavities. *Chem.* **2019**, *5*, 1167−1181.
(83) Du, M.; Martínez-Martínez, L. A.; Ribeiro, R. F.; Hu, Z.; Menon, V. M.; Yuen-Zhou, J. Theory for Polariton-Assisted Remote Energy Transfer. *Chem. Sci.* **2018**, *9*, 6659−6669.
(84) Gonzalez-Ballestero, C.; Feist, J.; Moreno, E.; Garcia-Vidal, F. J. Harvesting Excitons Through Plasmonic Strong Coupling. *Phys. Rev. B: Condens. Matter Mater. Phys.* **2015**, *92*, 121402.
(85) Bennett, K.; Kowalewski, M.; Mukamel, S. Novel Photochemistry of Molecular Polaritons in Optical Cavities. *Faraday Discuss.* **2016**, *194*, 259−282.
(86) Szidarovszky, T.; Halasz, G. J.; Csaszar, A. G.; Cederbaum, L. S.; Vibok, A. Conical Intersections Induced by Quantum Light: Field-Dressed Spectra from the Weak to the Ultrastrong Coupling Regimes. *J. Phys. Chem. Lett.* **2018**, *9*, 6215−6223.
(87) Gu, B.; Mukamel, S. Manipulating Nonadiabatic Conical Intersection Dynamics by Optical Cavities. *Chem. Sci.* **2020**, *11*, 1290−1298.
(88) Frisk Kockum, A.; Miranowicz, A.; De Liberato, S.; Savasta, S.; Nori, F. Ultrastrong Coupling Between Light and Matter. *Nature Rev. Phys.* **2019**, *1*, 19.
(89) Santhosh, K.; Bitton, O.; Chuntonov, L.; Haran, G. Vacuum Rabi Splitting in a Plasmonic Cavity at the Single Quantum Emitter Limit. *Nat. Commun.* **2016**, *7*, ncomms11823.
(90) Bitton, O.; Gupta, S. N.; Haran, G. Quantum Dot Plasmonics: From Weak to Strong Coupling. *Nanophotonics* **2019**, *8*, 559−575.
(91) Cohen-Tannoudji, C.; Dupont-Roc, J.; Grynberg, G. *Photons and Atoms: Introduction to Quantum Electrodynamics*; John Wiley & Sons, Inc.: Hoboken, NJ, 1989.
(92) Grynberg, G.; Aspect, A.; Fabre, C. *Introduction to Quantum Optics: From the Semi-classical Approach to Quantized Light*; Cambridge University Press: Cambridge, U.K., 2010.
(93) Steck, D. A. *Quantum and Atom Optics*. Available online at http://steck.us/teaching 2018.
(94) Rokaj, V.; Welakuh, D. M.; Ruggenthaler, M.; Rubio, A. Light−Matter Interaction in the Long-wavelength Limit: No Ground-State Without Dipole Self-Energy. *J. Phys. B: At., Mol. Opt. Phys.* **2018**, *51*, 034005.
(95) Schäfer, C.; Ruggenthaler, M.; Rubio, A. Ab initio nonrelativistic quantum electrodynamics: Bridging quantum chemistry and quantum optics from weak to strong coupling. *Phys. Rev. A: At., Mol., Opt. Phys.* **2018**, *98*, 043801.
(96) Vendrell, O. Coherent Dynamics in Cavity Femtochemistry: Application of the Multi-Configuration Time-Dependent Hartree Method. *Chem. Phys.* **2018**, *509*, 55−65.
(97) Flick, L. J.; Appel, H.; Ruggenthaler, M.; Rubio, A. Cavity Born−Oppenheimer Approximation for Correlated Electron−Nuclear-Photon Systems. *J. Chem. Theory Comput.* **2017**, *13*, 1616−1625.
(98) Lian, S.; Weinberg, D.; Harris, R.; Kodaimati, M.; Weiss, E. Subpicosecond Photoinduced Hole Transfer from a CdS Quantum Dot to a Molecular Acceptor Bound Through an Exciton-Delocalizing Ligand. *ACS Nano* **2016**, *10*, 6372−6382.
(99) Liu, C.; Qiu, F.; Peterson, J. J.; Krauss, T. D. Aqueous Photogeneration of H2 with CdSe Nanocrystals and Nickel Catalysts: Electron Transfer Dynamics. *J. Phys. Chem. B* **2015**, *119*, 7349−7357.
(100) Han, Z.; Qiu, F.; Eisenberg, R.; Holland, P. L.; Krauss, T. D. Robust Photogeneration of H2 in Water Using Semiconductor Nanocrystals and a Nickel Catalyst. *Science* **2012**, *338*, 1321−1324.
(101) Le Thomas, N.; Woggon, U.; Schöps, O.; Artemyev, M.; Kazes, M.; Banin, U. Cavity QED with Semiconductor Nanocrystals. *Nano Lett.* **2006**, *6*, 557−561.
(102) Gupta, S.; Waks, E. Spontaneous Emission Enhancement and Saturable Absorption of Colloidal Quantum Dots Coupled to Photonic Crystal Cavity. *Opt. Express* **2013**, *21*, 29612−29619.
(103) Gómez, D. E.; Vernon, K. C.; Mulvaney, P.; Davis, T. J. Surface Plasmon Mediated Strong Exciton-Photon Coupling in Semiconductor Nanocrystals. *Nano Lett.* **2010**, *10*, 274−278.
(104) Westmoreland, D. E.; McClelland, K. P.; Perez, K. A.; Schwabacher, J. C.; Zhang, Z.; Weiss, E. A. Properties of Quantum Dots Coupled to Plasmons and Optical Cavities. *J. Chem. Phys.* **2019**, *151*, 210901.
(105) Hu, J.; Li, L.-S.; Yang, W.; Manna, L.; Wang, L.-W.; Alivisatos, A. Linearly Polarized Emission From Colloidal Semiconductor Quantum Rods. *Science* **2001**, *292*, 2060−2063.
(106) Csehi, A.; Kowalewski, M.; Halász, G. J.; Vibók, Á. Ultrafast Dynamics in the Vicinity of Quantum Light-Induced Conical Intersections. *New J. Phys.* **2019**, *21*, 093040.

https://dx.doi.org/10.1021/acs.jpcb.0c03227
J. Phys. Chem. B XXXX, XXX, XXX−XXX

(107) Tvrdy, K.; Frantsuzov, P. A.; Kamat, P. V. Photoinduced Electron Transfer From Semiconductor Quantum Dots to Metal Oxide Nanoparticles. *Proc. Natl. Acad. Sci. U. S. A.* **2011**, *108*, 29−34.
(108) Tisdale, W. A.; Zhu, X.-Y. Artificial Atoms on Semiconductor Surfaces. *Proc. Natl. Acad. Sci. U. S. A.* **2011**, *108*, 965−970.
(109) Huo, P.; Miller, T. F., III; Coker, D. F. Communication: Predictive Partial Linearized Path Integral Simulation of Condensed Phase Electron Transfer Dynamics. *J. Chem. Phys.* **2013**, *139*, 151103.
(110) Caldeira, A. O.; Leggett, A. J. Influence of Dissipation on Quantum Tunneling in Macroscopic Systems. *Phys. Rev. Lett.* **1981**, *46*, 211−214.
(111) Braak, D. Integrability of the Rabi Model. *Phys. Rev. Lett.* **2011**, *107*, 100401.
(112) Chen, Q.-H.; Wang, C.; He, S.; Liu, T.; Wang, K.-L. Exact Solvability of the Quantum Rabi Model Using Bogoliubov Operators. *Phys. Rev. A: At., Mol., Opt. Phys.* **2012**, *86*, 023822.
(113) Zhong, H.; Xie, Q.; Batchelor, M. T.; Lee, C. Analytical Eigenstates for the Quantum Rabi Model. *J. Phys. A: Math. Theor.* **2013**, *46*, 415302.
(114) Groenhof, G.; Toppari, J. J. Coherent Light Harvesting through Strong Coupling to Confined Light. *J. Phys. Chem. Lett.* **2018**, *9*, 4848−4851.
(115) Luk, H. L.; Feist, J.; Toppari, J. J.; Groenhof, G. Multiscale Molecular Dynamics Simulations of Polaritonic Chemistry. *J. Chem. Theory Comput.* **2017**, *13*, 4324−4335.
(116) Xie, Q.; Zhong, H.; Batchelor, M. T.; Lee, C. The quantum Rabi model: solution and dynamics. *J. Phys. A: Math. Theor.* **2017**, *50*, 113001.
(117) George, J.; Chervy, T.; Shalabney, A.; Devaux, E.; Hiura, H.; Genet, C.; Ebbesen, T. W. Multiple Rabi Splittings under Ultrastrong Vibrational Coupling. *Phys. Rev. Lett.* **2016**, *117*, 153601.
(118) Todorov, Y.; Andrews, A. M.; Colombelli, R.; De Liberato, S.; Ciuti, C.; Klang, P.; Strasser, G.; Sirtori, C. Ultrastrong Light-Matter Coupling Regime with Polariton Dots. *Phys. Rev. Lett.* **2010**, *105*, 196402.
(119) Ciuti, C.; Bastard, G.; Carusotto, I. Ultrastrong Light-Matter Coupling Regime with Polariton Dots. *Phys. Rev. B: Condens. Matter Mater. Phys.* **2005**, *72*, 115303.
(120) De Bernardis, D.; Jaako, T.; Rabl, P. Cavity Quantum Electrodynamics in the Nonperturbative Regime. *Phys. Rev. A: At., Mol., Opt. Phys.* **2018**, *97*, 043820.
(121) Irish, E. K. Generalized Rotating-Wave Approximation for Arbitrarily Large Coupling. *Phys. Rev. Lett.* **2007**, *99*, 173601.
(122) Albert, V. V.; Scholes, G. D.; Brumer, P. Symmetric Rotating-Wave Approximation for the Generalized Single-Mode Spin-Boson System. *Phys. Rev. A: At., Mol., Opt. Phys.* **2011**, *84*, 042110.
(123) Yu, L.; Zhu, S.; Liang, Q.; Chen, G.; Jia, S. Analytical Solutions for the Rabi Model. *Phys. Rev. A: At., Mol., Opt. Phys.* **2012**, *86*, 015803.
(124) Wang, Y.; Haw, J. Y. Bridging the Gap Between the Jaynes-Cummings and Rabi Models Using an Intermediate Rotating Wave Approximation. *Phys. Lett. A* **2015**, *379*, 779−786.
(125) Yan, Y.; Lu, Z.; Zheng, H. Bloch−Siegert Shift of the Rabi Model. *Phys. Rev. A: At., Mol., Opt. Phys.* **2015**, *91*, 053834.
(126) Stokes, A.; Nazir, A. Gauge Ambiguities Imply Jaynes-Cummings Physics Remains Valid in Ultrastrong Coupling Qed. *Nat. Commun.* **2019**, *10*, 499.
(127) Müller, K.; Fischer, K. A.; Rundquist, A.; Dory, C.; Lagoudakis, K. G.; Sarmiento, T.; Kelaita, Y. A.; Borish, V.; Vučković, J. Ultrafast Polariton-Phonon Dynamics of Strongly Coupled Quantum Dot-Nanocavity Systems. *Phys. Rev. X* **2015**, *5*, 031006.
(128) Hennessy, K.; Badolato, A.; Winger, M.; Gerace, D.; Atatüre, M.; Gulde, S.; Fält, S.; Hu, E. L.; Imamoglu, A. Quantum Nature of a Strongly Coupled Single Quantum Dot−Cavity System. *Nature* **2007**, *445*, 896−899.
(129) Wang, W.; Watkins, N.; Yang, A.; Schaller, R. D.; Schatz, G. C.; Odom, T. W. Ultrafast Dynamics of Lattice Plasmon Lasers. *J. Phys. Chem. Lett.* **2019**, *10*, 3301−3306.
(130) Hohenester, U. Cavity Quantum Electrodynamics With Semiconductor Quantum Dots: Role of Phonon-Assisted Cavity Feeding. *Phys. Rev. B: Condens. Matter Mater. Phys.* **2010**, *81*, 155303.
(131) Hohenester, U.; Laucht, A.; Kaniber, M.; Hauke, N.; Neumann, A.; Mohtashami, A.; Seliger, M.; Bichler, M.; Finley, J. J. Phonon-Assisted Transitions From Quantum Dot Excitons to Cavity Photons. *Phys. Rev. B: Condens. Matter Mater. Phys.* **2009**, *80*, 201311.
(132) Majumdar, A.; Kim, E. D.; Gong, Y.; Bajcsy, M.; Vuckovic, J. Phonon Mediated Off-Resonant Quantum Dot−Cavity Coupling Under Resonant Excitation of the Quantum Dot. *Phys. Rev. B: Condens. Matter Mater. Phys.* **2011**, *84*, 085309.
(133) Fregoni, J.; Granucci, G.; Coccia, E.; Persico, M.; Corni, S. Manipulating Azobenzene Photoisomerization Through Strong Light-Molecule Coupling. *Nat. Commun.* **2018**, *9*, 4688.
(134) Groenhof, G.; Climent, C.; Feist, J.; Morozov, D.; Toppari, J. J. Tracking Polariton Relaxation with Multiscale Molecular Dynamics Simulations. *J. Phys. Chem. Lett.* **2019**, *10*, 5476−5483.
(135) del Pino, J.; Schroder, F.; Chin, A.; Feist, J.; Garcia-Vidal, F. Tensor Network Simulation of Polaron-Polaritons in Organic Microcavities. *Phys. Rev. B: Condens. Matter Mater. Phys.* **2018**, *98*, 165416.
(136) Virgili, T.; Coles, D.; Adawi, A. M.; Clark, C.; Michetti, P.; Rajendran, S. K.; Brida, D.; Polli, D.; Cerullo, G.; Lidzey, D. G. Ultrafast Polariton Relaxation Dynamics in an Organic Semiconductor Microcavity. *Phys. Rev. B: Condens. Matter Mater. Phys.* **2011**, *83*, 245309.
(137) Campos-Gonzalez-Angulo, J. A.; Ribeiro, R. F.; Yuen-Zhou, J. Resonant Catalysis of Thermally-Activated Chemical Reactions With Vibrational Polaritons. *Nat. Commun.* **2019**, *10*, 4685.
(138) Huo, P.; Coker, D. F. Communication: Partial Linearized Density Matrix Dynamics for Dissipative, Non-Adiabatic Quantum Evolution. *J. Chem. Phys.* **2011**, *135*, 201101.
(139) Lee, M. K.; Huo, P.; Coker, D. F. Semiclassical Path Integral Dynamics: Photosynthetic Energy Transfer with Realistic Environment Interactions. *Annu. Rev. Phys. Chem.* **2016**, *67*, 639−668.
(140) Castellanos, M. A.; Huo, P. Enhancing Singlet Fission Dynamics by Suppressing Destructive Interference between Charge-Transfer Pathways. *J. Phys. Chem. Lett.* **2017**, *8*, 2480−2488.
(141) Mandal, A.; Shakib, F. A.; Huo, P. Investigating Photoinduced Proton Coupled Electron Transfer Reaction Using Quasi Diabatic Dynamics Propagation. *J. Chem. Phys.* **2018**, *148*, 244102.
(142) Mandal, A.; Sandoval C., J. S.; Shakib, F. A.; Huo, P. Quasi-Diabatic Propagation Scheme for Direct Simulation of Proton Coupled Electron Transfer Reaction. *J. Phys. Chem. A* **2019**, *123*, 2470.
(143) Huo, P.; Miller, T. F. Electronic Coherence and the Kinetics of Inter-Complex Energy Transfer in Light-Harvesting Systems. *Phys. Chem. Chem. Phys.* **2015**, *17*, 30914−30924.
(144) Jain, A.; Subotnik, J. E. Does Nonadiabatic Transition State Theory Make Sense Without Decoherence? *J. Phys. Chem. Lett.* **2015**, *6*, 4809−4814.
(145) Jain, A.; Subotnik, J. E. Surface Hopping, Transition State Theory, and Decoherence. II. Thermal Rate Constants and Detailed Balance. *J. Chem. Phys.* **2015**, *143*, 134107.
(146) Takahashi, S.; Watanabe, K. Decoupling from a Thermal Bath via Molecular Polariton Formation. *J. Phys. Chem. Lett.* **2020**, *11*, 1349−1356.
(147) Di Stefano, O.; Settineri, A.; Macri, V.; Garziano, L.; Stassi, R.; Savasta, S.; Nori, F. Resolution of Gauge Ambiguities in Ultrastrong-Coupling Cavity Quantum Electrodynamics. *Nat. Phys.* **2019**, *15*, 803−808.
(148) De Bernardis, D.; Pilar, P.; Jaako, T.; De Liberato, S.; Rabl, P. Breakdown of Gauge Invariance in Ultrastrong-Coupling Cavity. *Phys. Rev. A: At., Mol., Opt. Phys.* **2018**, *98*, 053819.
(149) Göppert-Mayer, M. Elementary Processes With Two Quantum Transitions. *Ann. Phys. (Berlin, Ger.)* **2009**, *18*, 466−479.
(150) The strong coupling regime is commonly referred to as a Rabi frequency that is higher than all of the other decay rates of polariton, electronically (through nonradiative processes) or photonically (through radiative processes).

https://dx.doi.org/10.1021/acs.jpcb.0c03227
J. Phys. Chem. B XXXX, XXX, XXX−XXX